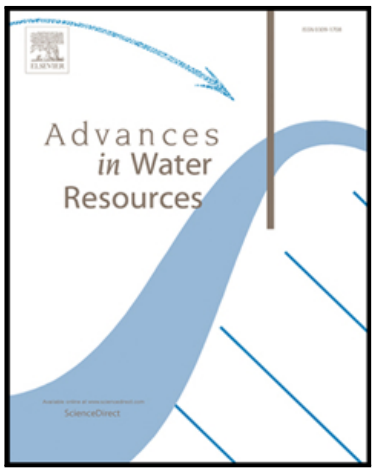

On the assimilation set-up of ASCAT soil moisture data for improving streamflow catchment simulation

Javier Loizu , Christian Massari , Jesús Álvarez-Mozos ,
Angelica Tarpanelli , Luca Brocca , Javier Casalí

PII: S0309-1708(16)30783-7
DOI: 10.1016/j.advwatres.2017.10.034
Reference: ADWR 2998

To appear in: *Advances in Water Resources*

Received date: 15 December 2016
Revised date: 27 October 2017
Accepted date: 28 October 2017

Please cite this article as: Javier Loizu , Christian Massari , Jesús Álvarez-Mozos , Angelica Tarpanelli , Luca Brocca , Javier Casalí , On the assimilation set-up of ASCAT soil moisture data for improving streamflow catchment simulation, *Advances in Water Resources* (2017), doi: 10.1016/j.advwatres.2017.10.034

Highlights

- ASCAT soil moisture data were assimilated into a conceptual and a physically-based model.
- Optimal EnKF assimilation set-ups improved streamflow simulation in Mediterranean catchments.
- Improvements varied from 6 to 45% from the validation run.
- Linear re-scaling method outperformed variance matching and cumulative distribution function.
- Largest improvements were achieved assuming observation errors within 1-6%.

Essential title page information

- **Title:**

On the assimilation set-up of ASCAT soil moisture data for improving streamflow catchment simulation

- **Author names (6) and affiliations.**

Javier Loizu[1]
Department of Projects and Rural Engineering. Public University of Navarre, Pamplona/Iruña, Navarre, Spain
javier.loizu@unavarra.es

Christian Massari[2]
Research Institute for Geo-Hydrological Protection, National Research Council, Perugia, Italy
christian.massari@irpi.cnr.it

Jesús Álvarez-Mozos[1]
Department of Projects and Rural Engineering. Public University of Navarre, Pamplona/Iruña, Navarre, Spain
jesus.alvarez@unavarra.es

Angelica Tarpanelli[2]
Research Institute for Geo-Hydrological Protection, National Research Council, Perugia, Italy
angelica.tarpanelli@irpi.cnr.it

Luca Brocca[2]
Research Institute for Geo-Hydrological Protection, National Research Council, Perugia, Italy
luca.brocca@irpi.cnr.it

Javier Casalí[1]
Department of Projects and Rural Engineering. Public University of Navarre, Pamplona/Iruña, Navarre, Spain
jcs@unavarra.es

- **Affiliations addresses:**

[1] *Public University of Navarre. Department of Projects and Rural Engineering. Laboratorio de Hidráulica, Edificio Los Olivos. Campus Arrosadía, 31006. Pamplona-Iruña, Navarra. Spain.*

[2] *Research Institute for Geo-Hydrological Protection, National Research Council. Via della Madonna Alta, 126. 06128, Perugia, Italy.*

- **Corresponding author:**

Javier Loizu[1]
Department of Projects and Rural Engineering. Public University of Navarre, Pamplona/Iruña, Navarre, Spain
Email: javier.loizu@unavarra.es

1. Introduction

Hydrological catchment models are useful tools that provide streamflow estimates for a wide range of applications including, among others, water resources management, civil engineering operations, climate change analysis, or bio-diversity conservation requirements. These models can differ

substantially in terms of the complexity of their structure, their level of parameterization, or their input requirements (Demaria et al., 2007); ranging from simple lumped conceptual models to largely parameterized, fully distributed physically based ones (Elsanabary and Gan, 2015). This variability can make some models more suitable for certain specific catchment characteristics (i.e., depending on the climatology or dominant runoff types in the catchment of interest) (Alvarez-Garreton et al., 2013).

A key issue affecting the efficiency of model predictions, regardless of the particular model type, is that they rely strongly on the optimal simulation of soil moisture conditions within the modeled catchment (Crow and Ryu, 2009). Surface Soil Moisture (SSM) is an important variable in the hydrological cycle that determines the partitioning of incoming water into infiltration and runoff, thus controlling runoff and baseflow generation from the soil profile, and determining river flows and flooding (Han et al., 2012). Currently, quantitative information on SSM can be obtained from spaceborne microwave instruments (Bartalis et al., 2007; Wanders et al., 2014a), allowing the integration of observed SSM data into hydrological models through Data Assimilation (DA) techniques, for more accurate streamflow prediction (Pauwels et al., 2002; Brocca et al., 2012; Alvarez-Garreton et al., 2015; Laiolo et al., 2015a; Leroux et al., 2016; López López et al., 2016). The selection of the optimal model for each specific catchment condition, along with an adequate Surface Soil Moisture Data Assimilation (SSM−DA) set-up is expected to provide a more realistic catchment modelling, leading to enhanced streamflow predictions. Some studies on SSM−DA focused on improving SSM model prediction (Crow and Reichle, 2008; Reichle et al., 2008; Ryu et al., 2009; Crow and Van Den Berg, 2010; Draper et al., 2012; Renzullo et al., 2014), while others evaluated whether SSM−DA also improved streamflow forecasts (Francois et al., 2003; Brocca et al., 2012, 2010b; Alvarez-Garreton et al., 2013; Alvarez-Garreton et al., 2014; Chen et al., 2014; Wanders et al., 2014b).

DA comprises different techniques applied to hydrology and other fields of science. Examples are: variational assimilation (Jazwinski, 1970), particle filtering (Gordon et al., 1993), or Kalman filtering (KF) (Kalman, 1960). Among them, the sequential type KF (Evensen, 1994) and its variants are the

DA methods most commonly used in SSM−DA. Several variants were developed from the original KF method to adapt it to different systems, in particular the ensemble Kalman filter (EnKF) (Evensen, 1994) was developed to address nonlinear model dynamics without linearizing model equations. The EnKF has been frequently used to assimilate observations into hydrological models because it is well-suited to highly dimensional nonlinear systems (Wanders et al., 2014b), and it is computationally efficient and easy to implement (Reichle et al., 2002; Crow and Wood, 2003; Pauwels et al., 2007). The EnKF propagates an ensemble of model realizations generated by perturbing model input values. The error background covariance matrix is then estimated from the ensemble statistics (Trudel et al., 2014), where the probability density of the model states is represented by an ensemble where the mean is the best estimate (Gaussian assumption), and the ensemble spread defines the error variance (Xu et al., 2015).

Different sources of observed SSM have become available in the last years, acquired mostly from sensors operating in the low frequency microwave region from 1 to 10 GHz (Albergel et al., 2012), which differ in their sensing mode (active or passive), frequency, and retrieval algorithm (Rötzer et al., 2014). Different passive microwave sensors have been observing the Earth for the last decades (e.g. Soil Moisture and Ocean Salinity mission (SMOS) (Kerr et al., 2010), NASA's Soil Moisture Active Passive (SMAP) (Entekhabi et al., 2010) or the Advanced Microwave Scanning Radiometer, AMSR-E (Owe et al., 2008)) providing a quasi-continuous global dataset since 1978 (Liu et al., 2012). These passive systems are less sensitive to the effects of surface roughness and vegetation structure with respect to active ones and have a larger soil penetration depth in the case of L-Band radiometers like SMOS and SMAP (3-5 cm, Rötzer et al., 2014). On the other hand, active microwave sensors (i.e., scatterometers) have been frequently used in SSM−DA because of their relatively good accuracy (Brocca et al., 2011b) and their long temporal coverage (i.e., since 1991, Wagner et al., 2013). Among these, the Advanced Scatterometer (ASCAT) (launched in 2006) was the first to provide an operational near real-time (NRT) Level 2 SSM product (Albergel et al., 2012). Its operating C-band frequency provides higher spatial resolution and is less affected by radiofrequency interferences but has a lower soil penetration depth (0.5-2 cm).

When diverse sensors and models are used to explore a geophysical target (i.e. SSM), it is important to investigate how information from multiple sources can be compared and/or integrated. In particular, one of the main challenges faced by SSM−DA is that model simulations and satellite retrievals often exhibit differences in SSM patterns, mainly in terms of different time series mean values and variation ranges (Chen et al., 2011). Two main causes can be identified as the factors producing those differences: (1) the difference between satellite penetration, which depends on the frequency of the sensor (Paulik et al., 2014), and the model representation of SSM (soil layers configuration and depth); and (2) the inherent systematical differences coming from the estimation of the same physical variable with different techniques (i.e. model and sensor retrievals) (Dorigo et al., 2015). These two causes need to be addressed differently. The first is normally addressed by making both time series represent the same physical variable by transferring satellite information to the root zone, or to the depth of the modelled surface layer, by using filtering techniques, such as the Soil Water Index (SWI) (Wagner et al., 1999). The second cause is addressed by using re-scaling techniques (RTs) that mitigate any systematic differences between model simulations and SSM observations, so that these representativeness issues are solved (Lievens et al., 2016) and the resulting re-scaled SSM time-series can be useful in terms of its variability (not its absolute values) (Kumar et al., 2012).

Different RTs exist, depending on the number of statistical moments that are matched between observed (SWI) and simulated SSM time-series. The most commonly applied RTs are (López López et al., 2016): (1) the linear re-scaling (LR) (Brocca et al., 2011a), where only the mean value of the observations/SWI is adjusted; (2) the mean and standard deviation matching, named Variance Matching method (VM) (Draper et al., 2009); and (3) the cumulative distribution function (CDF) matching (Reichle and Koster, 2004) which assures an all order moment matching. Re-scaling strongly affects the outcome of SSM−DA, making this a very active field of research (Ryu et al., 2009; Wanders et al., 2012; Alvarez-Garreton et al., 2014; Paulik et al., 2014; Massari et al., 2015; Xu et al., 2015).

The retrieval of SSM is affected by several error sources that degrade to a certain extent the final SSM estimate (Su et al., 2014). Thus, typical hydrological applications such as calibration, validation, bias correction, or data assimilation can only be performed properly when the error statistics in the data and their relationships are known (Su et al., 2014). This influences notably DA, as the observation error assumed for SSM products has also a strong influence on the SSM−DA results.

Although operational products, such as ASCAT−SSM, provide a nominal observation error as ancillary information with the SSM estimate, this value may vary largely depending on the area (e.g., land cover and topography) and the surface conditions as demonstrated by many validation studies (Albergel et al., 2009; Brocca et al., 2010a; Hahn et al., 2012; Leroux et al., 2014; Paulik et al., 2014; Bhimala and Goswami, 2015). For instance, the ASCAT−SSM product has been extensively validated over several instrumented test sites located in different climatic regions with different land cover (Wagner et al., 2013) providing root mean square error (RMSE) values spreading around 0.04 $m^3 m^{-3}$ (Brocca et al., 2011; Matgen et al., 2012b; Wagner et al., 2013) which correspond to the accuracy goal of both the SMOS and SMAP missions. This error estimate could be potentially used as an observation error estimate within DA experiments when no ground reference is available at a particular site, but it could not guarantee optimal results. To overcome this issue, many studies (Dorigo et al., 2010, 2015; Chen et al., 2014; Renzullo et al., 2014; Su and Ryu, 2015; Alvarez-Garreton et al., 2016) proposed to use Triple Collocation (TC) (Stoffelen, 1998) for characterizing the error variance of three collocated soil moisture data sets along with the affine parameters that characterize the biases, which can be a valid solution for selecting a reliable SSM error in absence of a ground reference. However, despite successfully applied in different studies, this technique is also subjected to some restrictions related to the underlying assumptions of the method, which need to be preserved when the method is to be applied (e.g., non-zero error cross correlations among the products, stationarity and linearity among the three estimates) (Su et al., 2014). Hence, the optimization of the observation error to each specific catchment and model conditions as in Massari et al. (2015) might be a valuable solution for optimally assimilating SSM into a hydrological model.

In the few last years, SSM−DA techniques have been applied to catchments of contrasting rainfall regimes, ranging from semi-arid (<400 mm/year) (Alvarez-Garreton et al., 2015; 2014; Lievens et al., 2015) to intermediate (Brocca et al., 2012) or humid ones (> 1000 mm/year) (Brocca et al., 2010b). In addition, different model types have been used for SSM−DA, ranging from simple lumped conceptual models (Francois et al., 2003) to complex, physically based models (Pauwels et al., 2002; Chen et al., 2011) and fully distributed models of different levels of complexity (Wanders et al., 2014b; Lievens et al., 2015). However, the degree of improvement in streamflow predictions varied significantly, from no improvement (Han et al., 2012), to limited improvement (Lievens et al., 2015) or up to 10-30 % improvements (Brocca et al., 2012; Matgen et al., 2012a; Massari et al., 2015). Furthermore, ASCAT SSM data were successfully assimilated in Mediterranean catchments, as shown in Cenci et al. (2016). All these studies are difficult to compare, interpret and generalize because their results depend largely on model structure and catchment characteristics, mainly their rainfall regime, and thus on the dominant runoff mechanisms (Lievens et al., 2015). While streamflow assimilation based on two models of different conceptualization (distributed and physically based vs lumped) has been tested using the same catchments (Randrianasolo et al., 2014), to our knowledge, this type of study has not been performed for remotely sensed SSM−DA, except in one isolated case where ASCAT-SSM was assimilated into the MISDc model (Brocca et al., 2011b) considering a one-layer and a two-layers scheme. Therefore, it would be interesting to have a comparison of the SSM−DA performance of models of varying structure and conceptualization (conceptual and physically-based) applied to the same catchments.

The following research questions define the objectives of this study:

- Can the assimilation of ASCAT data, by using the EnKF, improve hourly streamflow prediction?
- Do the re-scaling techniques have a significant influence on the DA results?
- Does the assumed SSM observation error have a significant influence on the DA results?
- Which is the DA performance when different conceptual and physically-based models are used?

Given these objectives, ASCAT−SSM data are assimilated through the EnKF into two models of contrasting structure and over two different catchments. The eventual benefits of SSM−DA with respect to validated streamflow forecasts are assessed at an hourly and monthly scale. The influence of re-scaling techniques and observation error optimization on the outcomes of SSM−DA are also discussed. It must be pointed out that the relatively long period of analysis (11 years) allows us to perform a clear and rigorous separation between calibration and validation steps. This allows to test the potential impact of the stationarity of the observation error and of the bias on the optimality of the assimilation results during the validation period. Altogether, this study addresses the existing demand for more real-case studies (Alvarez-Garreton et al., 2014) that contribute to build evidence and understanding of the improvement skill of SSM−DA over a wide range of catchment characteristics.

2. Study sites and soil moisture dataset

2.1. Studied catchments

2.1.1. Nestore catchment

The Nestore catchment (725 km^2) is located in the upper Tiber river catchment, an area with a complex topography prone to widespread frontal rainfall that causes major flood events. The main land uses are grasslands (54 %) and woods (38 %), whereas urban areas cover only a small part (5 %) of the catchment. The geology is characterized by terrigenous facies and flysch deposits. The soil, overlying practically impervious rocks, contains clay and sandy silt. Further information on the soil hydrological properties can be found in Massari et al. (2015). The climate is Mediterranean, with a mean annual rainfall of 740 mm. The mean slope of the catchment is 17 %. The highest monthly rainfall values generally occur during the autumn-winter period, when floods, caused by widespread rainfall, normally occur. A dense, real-time hydrometeorological network (1 station every 150 km^2) has been operating in the area for more than 20 years, and the data are recorded with a time interval of 30 min. Streamflow is measured at the gauging station of Marsciano (Fig. 1).

Figure 1

2.1.2. Arga catchment

The Arga river is one of the main tributaries of Ebro, whose basin covers most of northeastern Spain. Only its upper part was used in this study, specifically the 810 km^2 defined by the gauging station in the municipality of Arazuri (Fig. 1). At this point, the Arga river has a main river channel that is 53 km long. In this study, a 69-km^2 subcatchment feeding a reservoir (Eugi) in the northern boundary of the catchment was subtracted. Thus, both rainfall and streamflow measured at the reservoir's outlet were removed from the analysis, and an effective catchment area of 741 km^2 was finally used. The predominant land covers in the catchment are forest (46 %, mostly in the northern part), rainfed cereal crops (33 %), bushes (12 %) and urban areas (10 %). In the southern half of the catchment, the predominant soils belong to the *Xerorthent* group (NRCS-USDA, 2014), have a silty-clay-loam texture, and are more than 1 m deep except for those on the eroded hillslopes that are shallow. Mean annual rainfall is 956 mm, and the climate in the area is mild-humid Mediterranean. The mean slope is 24 %. Arga catchment is heavily instrumented, with 21 measuring stations (Fig. 1) observing meteorological data in the area since 1975. Twelve of these stations are managed manually on a daily basis, and nine are automatic with a 10-minute recording interval. A more detailed description of the catchment can be found in Loizu et al. (2016).

2.2. Surface soil moisture satellite data

ASCAT is a scatterometer that operates in the C-band (5.255 GHz) at VV polarization and scans the Earth's surface in descending and ascending overpasses (Bartalis et al., 2007; Zeng et al., 2015). It was first installed onboard of the Meteorological Operation-A (MetOp-A, launched in 2006) satellite, and then on the other two satellites of the series: MetOp-B (launched in 2012), and MetOp-C (scheduled for launch in 2018), which are expected to provide an uninterrupted stream of ASCAT backscatter observations well into the 2020s (Wagner et al., 2013). The MetOp-A satellite follows a near-polar sun-synchronous orbit at an altitude of approximately 817 km with a repeat cycle of 29 days, completing 14 orbits per day and providing a daily global coverage of approximately 82 % of the Earth. Measurements of western Europe are generally obtained twice a day: in the morning

(descending pass) and in the evening (ascending pass), between 08:00-11:00 and 17:00-21:00 UTC, respectively (Brocca et al., 2010b). SSM products are available with a spatial resolution of 50 km and 25 km (resampled to 25-km and 12.5-km grids in the swath geometry).

The ASCAT-SSM product represents the degree of saturation of the topmost soil layer, ranging from 0 % (dry) to 100 % (wet) (Albergel et al., 2012). To retrieve SSM, the backscattering coefficients are first normalized to a reference incidence angle of 40º and then scaled between the lowest and highest values measured over a long period (Bartalis et al., 2007; Parrens et al., 2012). The soil moisture retrieval scheme uses a change detection model that is very similar in functionality to the Water Cloud Model (Attema and Ulaby, 1978; Bartalis et al., 2007). Two different ASCAT-derived SSM products are available. The first one is generated by the European Organisation for the Exploitation of Meteorological Satellites (EUMETSAT) (Wagner et al., 2013), and it is distributed in NRT. The second one is calculated and distributed by the TU-Wien and includes most recent algorithmic updates, product reprocessing and updating (Naeimi et al., 2009). The TU-Wien product was used in this study and consists of a 6-year (2007-2012) time series at a 25-km resolution (resampled to 12.5 km). The RMSE of the ASCAT−SSM product is estimated to range between 0.014 and 0.06 $m^3 m^{-3}$, according to different validation studies performed worldwide (Albergel et al., 2009; Brocca et al., 2010; Matgen et al., 2012b), with an expected mean value of 0.04 $m^3 m^{-3}$ (Matgen et al., 2012a).

Figure. 2.

The mean SSM value of four pixels were used (2223595, 2218893, 2218897 and 2214191) for the Nestore catchment, whereas six pixels (2218622, 2218618, 2213916, 2213912, 2209202, and 2209198) were considered for Arga (Fig. 2). In this research, a total study period of 11 years (Oct 2001 - Oct 2012) was considered for both catchments.

3. Methodology

3.1. Hydrological catchment models

Two models of different complexity and structure were used: *Modello Idrologico Semi-Distribuito in continuo* (MISDc) (Brocca et al., 2011b), and *TOPMODEL-based Land-Atmosphere Transfer Scheme* (TOPLATS) (Famiglietti and Wood, 1994; Peters-Lidard et al., 1997) (Fig. 3).

Figure. 3.

3.1.1. MISDc model

MISDc is a conceptual and semi-distributed model that consists of two main components, a soil water balance model (SWB) (Brocca et al., 2008) to simulate the soil moisture temporal pattern, and a routing module (Melone et al., 2001) for transferring the rainfall excess to the catchment outlet. The two components are linked through an experimentally derived linear relationship (Brocca et al., 2009b) between the potential maximum soil moisture retention (*S*) of the Soil Conservation Service-Curve Number (SCS-CN) (SCS, 1972) and the relative soil moisture at the beginning of the event (Fig. 3b). The SWB model is a simple model that simulates the main processes in a single soil layer (i.e., infiltration, percolation and evapotranspiration). In particular, infiltration is modeled through the Green–Ampt equation, drainage is modeled using a gravity-driven non-linear relationship, and actual evapotranspiration is modeled using a linear relationship with potential evapotranspiration, calculated using a modified Blaney and Criddle method (Blaney and Criddle, 1950). Once the *S* parameter is estimated, the routing to the catchment outlet is obtained from the convolution of the rainfall excess and the geomorphological instantaneous unit hydrograph (GIUH) proposed by Gupta et al. (1980) (Fig 3c). The model was developed as a single layer soil simulation structure, which is the version used in this study (Fig 3a). MISDc was also implemented with a second layer for a specific study to improve the soil water balance simulation, with the objective of making it a suitable tool to adequately assimilate satellite SSM observations, but that 2 layers configuration did not improve DA performance (Brocca et al., 2012), and hence, the 1 layer version was used here.

The meteorological forcing required by MISDc as input are rainfall and air temperature, and it provides the saturation degree and the discharge as output data. To run the model, 9 parameters have to be estimated, some are physical parameters (i.e., saturated hydraulic conductivity (K_s), pore size distribution index (β), and maximum water capacity of the soil layer (W_{max})), and some empirical (i.e., the parameter controlling the fraction of drainage that transforms into subsurface runoff (v), the correction coefficient for potential evapotranspiration (K_c), the lag-area relationship parameter (η), the initial abstraction coefficient (λ) and the parameter of the relationship between modeled SM and the S of the SCS-CN method (α)).

MISDc has been successfully applied to many catchments worldwide (Masseroni et al., 2017), including the Tiber River in central Italy (Brocca et al., 2011b), for flood prediction and operational purposes. Further descriptions of the model and its performance under Mediterranean conditions can be found in Camici et al. (2011), Brocca et al. (2013), and Massari et al. (2015). Specific DA studies using MISDc include Brocca et al. (2010; 2012). In this research, the model has been applied in a lumped mode, with an hourly time-step and the calibration was performed using a standard gradient-based automatic optimization search function (Brocca et al., 2011), tuning four parameters (W_{max}, K_s, K_c and η) and considering the period Oct 2001 - Dec 2009 for calibration and Jan 2010 - Oct 2012 for validation. Further details on MISDc are provided in Brocca et al. (2011b).

3.1.2. TOPLATS model

The second model, TOPLATS, is based on the TOPMODEL approach (Beven and Kirkby, 1979), which is a contributing-area conceptual model where the predominant factors determining the formation of runoff are represented by the topography of the catchment and a negative exponential law linking the transmissivity of the soil with the vertical distance from the ground level (Franchini et al., 1996). This initial conceptualization was later added a Soil-Vegetation-Atmosphere-Transfer (SVAT) scheme (Famiglietti and Wood, 1994) that initialized the development of a full hydrological catchment model (Fig. 3a). It then incorporated separate computations of water and energy balances. The initial configuration of TOPLATS was later improved by Peters-Lidard et al. (1997) and by Pauwels and

Wood (1999). The main concept in TOPLATS is that shallow groundwater gradients, estimated from the local topography through a topographic index (TI) (Sivapalan et al., 1987), set up spatial patterns of soil moisture that control infiltration and runoff generation during storm events and evaporation and drainage during inter-storm periods. The model can be run as a fully distributed model or in a statistical (semi-distributed) mode. In the statistical mode, the one used in this study, TI is represented through its statistical probability distribution given a fixed bin-size (Fig. 3b). TOPLATS simulates three processes for streamflow generation: infiltration excess, saturation excess and baseflow. Separate routing routines were added to the model, based on the unit hydrograph method proposed by the SCS (Soil Conservation Service, 1972) (Fig. 3c).

The model divides the soil column into two layers: a thin surface zone (SZ), of a user-defined permanent depth (in this work 5 cm), and a deeper transmission zone (TZ) that represents the soil depth between the SZ and the water table (WT). In TOPLATS, the soil properties are modeled through the closed-form analytical equations of Brooks and Corey (1964), which express the relationship between the soil moisture content (θ), the hydraulic head (ψ) and the hydraulic conductivity (K_s) (Loosvelt et al., 2014). The interception capacity of the canopy is calculated as a function of the leaf area index (LAI) (Dickinson, 1984), and infiltration is calculated as the minimum of the soil infiltration capacity (Philip, 1957; Milly, 1986) and net precipitation. The exchange of soil water between the upper and lower layers is calculated assuming diffusive flux (Peters-Lidard et al., 1997), where diffusivity is controlled by Brooks and Corey (1964) parameters. Evaporation is calculated with a soil resistance formulation (Passerat De Silans et al., 1986). In TOPLATS, the vegetation properties and their growing cycle are controlled by a significant number of parameters (e.g., LAI, albedo, emissivity, roughness length for heat and momentum transfer, maximum and minimum stomatal resistance, etc.). Specifically, in this study, plant growth was modelled by a monthly update of the different mentioned parameters for the main vegetation classes (i.e. rain-fed cereal, irrigated crops and forests), as explained in Loizu et al. (2016). TOPLATS requires seven climate variables as input: temperature, relative humidity, atmospheric pressure, wind speed, rainfall rate, and longwave and shortwave downwards radiations.

TOPLATS was calibrated through a multi-start optimization approach combined with an automatic search minimization algorithm (Loizu et al., 2016), tuning six parameters (Brooks-Corey pore size distribution index (*B)*, bubbling pressure (ψ_c), saturated soil moisture (θ_s), hydraulic conductivity (K_s), subsurface flow at complete saturation (Q_0) and hydraulic conductivity decay (*f*)). TOPLATS was also run in hourly basis, and the Oct 2001 - Dec 2009 period was used for calibration and Jan 2010 - Oct 2012 for validation. Different types of remotely sensed information have been assimilated into TOPLATS for improving soil moisture (Houser et al., 1998; Crow et al., 2001; Lucau-Danila et al., 2005) or streamflow simulation (Pauwels et al., 2001, 2002). A review on the studies carried out using TOPLATS was presented in Loizu et al. (2016).

3.2. ASCAT−SSM preprocessing: soil water index (SWI) and re-scaling methods

To solve the mismatch between ASCAT sensing depth and that of the surface layer considered by the models, ASCAT−SSM values were subjected to two pre-processing steps: the soil water index (SWI) calculation and the SWI re-scaling (Brocca et al., 2009a; Matgen et al., 2012b; Alvarez-Garreton et al., 2014, 2015; Paulik et al., 2014; Cho et al., 2015)**.** For the SWI calculation, a recursive filter was used (Wagner et al. 1999), which depends on a single parameter, *T*, characterizing the temporal variation of SM within the root-zone profile (Brocca et al., 2012). It works as a low-pass filter that smoothens the SSM series (Matgen et al., 2012b) by assuming a linear relationship between the SM in the first centimeters of the soil and the SM content in the deeper root zone (Alvarez-Garreton et al., 2014). The recursive filter (Eq. 1) at each time step (*k*) is calculated as follows (Albergel et al., 2008):

$$SWI_k = SWI_{k-1} + U_k\,[O_k - SWI_{k-1}] \quad (1)$$

where O_k is an available ASCAT observation and U_k is a gain updating term (Eq. 2), varying between 0 and 1, calculated as:

$$U_k = \frac{U_{k-1}}{U_{k-1} + e^{-\left(\frac{k-(k-1)}{T}\right)}} \quad (2)$$

The parameter *T* was calibrated (considering a variation range between 1 and 200 days) by maximizing the correlation coefficient (R) between the generated SWI and the model-simulated SSM time series. This calibration was performed for a 2-year period: Jan 2007 - Jan 2009.

In a second step, SWI values were re-scaled through different RTs. Three different RTs were selected, and their influence on the DA results was evaluated. These methods were selected to cover a wide range of order – statistical – moments rescaling (as in Lievens et al., 2015):

- **Linear regression (LR).** In this approach, minimization of the mean square difference (*msd*) between modeled and rescaled data is performed (Yilmaz and Crow, 2013) through a least squares linear regression technique (Crow et al., 2005; Alvarez-Garreton et al., 2014). This method matches the mean values of simulated and observed (SWI) data.
- **Variance matching (VM).** This method involves re-scaling the observed SSM values to match the first two moments (mean and variance) of the probability distribution of the simulated time series (Crow et al., 2005; Sahoo et al., 2013; Lievens et al., 2015; Massari et al., 2015).
- **Cumulative distribution function matching (CDF).** This method was first proposed by Reichle (2004) and has been applied in different assimilation and SSM product evaluation experiments (Drusch, 2005; Scipal et al., 2008; Matgen et al., 2012b; Liu et al., 2012; Alvarez-Garreton et al., 2014; Massari et al., 2015). CDF matching ensures that the statistical distribution of both the satellite data and modelled time series is the same, so that assimilation only adjusts the model for random variations (Renzullo et al., 2014).

The three RTs were first fitted using a 3-year (Jan 2007-Dec 2009) calibration period and then validated using a 2-year and 9-month period (Jan 2010 to Oct 2012). This setup guarantees that re-scaling is always based on previous data; consequently, DA can be performed in real time, similarly to Alvarez-Garreton et al. (2014).

3.3. Ensemble Kalman filter (EnKF)

The EnKF (Evensen, 2003) is a Monte Carlo-based approach allowing model uncertainties to be calculated from the ensemble spread, that is assumed to be large enough to represent the true

uncertainty of the simulation (Wanders et al., 2014a). The EnKF takes advantage of a statistical approach to evaluate the error covariance matrices of the Kalman filter equations.

In the EnKF, the background state vector becomes an *n* (state variables) x N_r (ensemble members) background matrix (X^b) needed to derive the model error matrix (Thiboult and Anctil, 2015), where: $X^b = \left(X_1^b, \dots, X_{Nr}^b\right)$, and where each ensemble member's state variables are defined as: $X_i^b = \left(x_1^b, x_2^b, \dots, x_n^b\right)_i^T$. As the real true state is unknown, it is approximated by the ensemble mean ($\bar{x}^b$), where *i* refers to the i-*th* member:

$$\bar{x}^b = \frac{1}{N_r} \sum_{i=1}^{Nr} X_i^b \quad (3)$$

In this study, the state variables contained in the state matrix were the Surface Zone (upper layer) soil moisture content in TOPLATS model and the relative soil water content [0-1] of the only layer in MISDc. In TOPLATS, the SM content corrections performed in the SZ through EnKF-DA, are rapidly transferred by the model itself to the lower TZ layer, and impact the runoff mechanisms within the model as these corrections also influence the water table depth. This approach, updating only the upper layer of the model, was selected for this study as it allowed to fix the depth of the upper layer to a similar depth of that of the ASCAT observations.

From the ensemble perturbation matrix, defined as $X'^b = X_i^b - \bar{X}^b$, the ensemble background error covariance matrix (*P*) is obtained as in Eq. 4.

$$P = \frac{1}{N_r - 1} x'^b x'^{bT} \quad (4)$$

On the observation side, uncertainty is considered and evaluated through perturbed observations. An *m* x *N* matrix, where *m* is the number of observations, needs to be calculated to represent perturbed observations ($y_i = y + \varepsilon_i^o$). The perturbations ensemble ($E = [\varepsilon_1^o, \varepsilon_2^o, \dots, \varepsilon_{Nr}^o]$) is generated with an ensemble mean equal to zero (Trudel et al., 2014), and the ensemble representation of the observation error covariance matrix (*Z*) is then defined as:

$$Z = \frac{1}{N_r - 1} EE^T \quad (5)$$

The Kalman gain (G_k) (Eq. 6), at each time step *k*, represents the relative importance of the observation error with respect to the prior estimate (i.e., model simulation) and acts as a weighting

coefficient. Z_k denotes the covariance of the observational noise (Thiboult and Anctil, 2015) at time step k, P_k accounts for model uncertainty, and H_k is the observation operator (SWI vector in this study). G_k is thus calculated as:

$$G_k = P_k H_k^T \left(Z_k + H_k P_k H_k^T\right)^{-1} \quad (6)$$

ASCAT SSM observation error was optimized as in Massari et al. (2015), in order to pick up the observation error value that provides the best streamflow simulation within the DA experiment. For this, ten different ASCAT observation error values were considered: 0.01, 0.1, 1, 2, 4, 6, 8, 10, 15 and 20 %, based on previous studies (e.g., Brocca et al. (2010), who estimated a 10 % error in SWI values obtained from ASCAT data, in a validation study based on in-situ observations). Then, the Kalman gain was calculated with each of these values and subsequently ASCAT SSM was assimilated. This way, the error value yielding the best streamflow prediction after SSM assimilation was obtained for each catchment and model combination.

In the last step of the assimilation algorithm, the new model state matrix (x_k^a) is updated (Eq. 7) based on an a priori (forecasted) model state matrix (x_k^b), the Kalman gain (G_k), and the deviation between measured and predicted observations (Abaza et al., 2015).

$$x_k^a = x_k^b + G_k\left(y_k - H_k\left[x_k^b\right]\right) \quad (7)$$

The EnKF has been successfully used in different hydrological applications, including streamflow prediction, through assimilation of soil moisture and streamflow data (Xie and Zhang, 2010; Li et al., 2014; Trudel et al., 2014; Wanders et al., 2014b; Abaza et al., 2015).

3.4. Ensemble verification criteria

The EnKF requires the generated ensemble to comply with certain spread characteristics, i.e., to generate a meaningful ensemble that represents the uncertainty of each hydrological model's forecasts (Matgen et al., 2012a). For that, the standard deviation of the perturbations must be gradually increased until the ensemble mean differs from the observation by a value that is equal to the time average of the ensemble spread, and so the observed trend is statistically indistinguishable from a

member of the ensemble (Pauwels and De Lannoy, 2009; Matgen et al., 2012a)**.** Following those guidelines, in this study the ensemble of model simulations was obtained by perturbing two input variables (rainfall and temperature) and the three most sensitive parameters of each model, previously identified through sensitivity analyses. The parameters perturbed in MISDc were W_{max}, K_s and K_c, while in TOPLATS they were B, ψ_c and f.

An ensemble of 50 members was created by perturbing the rainfall and temperature input data, as well as the most sensitive parameters. This ensemble size can be considered sufficiently consistent (Moradkhani et al., 2005) to adequately depict the uncertainty contained in the observation of climatic variables, and on model's structure and parameterization, without compromising the efficiency of the procedure in terms of computational time-consumption. Temperature was perturbed with a zero-mean additive Gaussian noise, whereas a Log-normal multiplicative noise was added to rainfall in MISDc (Chen et al., 2011), and a Gamma function multiplicative noise was added to rainfall in TOPLATS. Both multiplicative functions provide a very similar type of perturbation. On the other hand, model parameters were perturbed by adding them a multiplicative random Gaussian noise (Brocca et al., 2010b; Alvarez-Garreton et al., 2015), which was set as a fraction of their calibrated values. In each case, the intensity of the perturbation was set through the standard deviation (STD) of the added noise. To ensure that the created ensemble was meaningful, that is, it adequately represented modeling uncertainty, three ensemble characteristics (Eq. 8, 9 and 10) were calculated: (1) the ensemble spread ($ensp_k$), (2) the ensemble mean square error (mse_k), and (3) the ensemble skill ($ensk_k$):

$$ensp_k = \frac{1}{N_r}\sum_{i=1}^{N_r}\left(S_k^i - \overline{S_k^i}\right)^2 \quad (8)$$

$$mse_k = \frac{1}{N_r}\sum_{i=1}^{N_r}\left(S_k^i - O_k^i\right)^2 \quad (9)$$

$$ensk_k = \left(\overline{S_k} - O_k\right)^2 \quad (10)$$

where k indicates the specific time-step of the observed (O) and simulated (S) time series, Nr is the ensemble size, and an overbar indicates the mean over the ensemble. These features were first computed at each time step (k) and then averaged over the evaluated period. Two conditions must be met by the ensemble (De Lannoy et al., 2006; Brocca et al., 2012; Matgen et al., 2012a; Plaza et al., 2012; Alvarez-Garreton et al., 2014); first, to ensure that the ensemble spread is large enough, the

temporal average of the ensemble skill should be similar to the temporal average of the ensemble spread (De Lannoy et al., 2006; Alvarez-Garreton et al., 2014) (Eq. 11):

$$\frac{\langle ensk \rangle}{\langle ensp \rangle} \approx 1 \quad (11)$$

where ‹ › indicates the average over the simulation period. Values larger than 1 indicate spreads that are too small if the model is not biased (De Lannoy et al., 2006). Secondly, Eq. 12 must be validated to check that the truth (observed streamflow) is statistically indistinguishable from a member of the ensemble (De Lannoy et al., 2006; Matgen et al., 2012a).

$$\frac{\langle \sqrt{ensk} \rangle}{\langle \sqrt{mse} \rangle} \approx \sqrt{\frac{N_r + 1}{2N_r}} \quad (12)$$

Ten different combinations of STD values for parameter and climate variables perturbations were tested for the ensemble generation, and the combination providing the closest results to the two validation criteria was selected. Specifically, to generate the ensemble in Nestore, the designated MISDc parameters were perturbed with a multiplicative noise characterized by mean equal to 1 and STD ranging from 0.3 to 0.8 (different STD were applied to each parameter, within the shown range). For TOPLATS all the parameters were perturbed with the same STD-noise, equal to 0.15. Rainfall was perturbed with a multiplicative noise of STD = 0.25 in MISDc and 0.9 in TOPLATS. For Arga catchment the STD of the parameters' noise ranged between 0.1 and 0.8 for MISDc and was taken equal to 0.25 for TOPLATS; rainfall was perturbed with a STD-noise of 1.2 in MISDc and 2.8 in TOPLATS. Finally, for the temperature an additive noise of STD = 3.0 in MISDc, and STD = 2.0 in TOPLATS was used.

3.5. Performance indices

The model performance was evaluated through five different statistical measures, including three efficiency measures (*NSE*, Eff_{Val} and Eff_{OL}), the percentage of volumetric error (*Pbias*) and the normalized RMSE (*NRMSE*).

The first efficiency criterion used was the Nash-Sutcliffe efficiency (NSE) (Nash and Sutcliffe, 1970), which measures the fraction of the observed streamflow variance explained by the model, calculated

as the magnitude of the residual variance (noise) relative to the observed variance (information). Its optimal value is 1. NSE was calculated following Eq. 13.

$$NSE = 1 - \frac{\sum_{k=1}^{Pa}\left(Q_{obs}(k) - Q_{TS}(k)\right)^2}{\sum_{k=1}^{Pa}(Q_{obs}(k) - \overline{Q_{obs}})^2} \quad (13)$$

where P_a is the length of the discharge time series, k each time-step, Q_{obs} is the observed discharge, Q_{TS} is the simulated discharge, and $\overline{Q_{obs}}$ is the mean value of the observed discharge. NSE focuses on the simulation performance of high flows. In Eqs. 13 and 14 the subscript TS refers to any of the different time-series performance evaluated in this study, namely: calibration (Q_{Cal}), validation (Q_{Val}), open loop (Q_{OL}) or data assimilation (Q_{DA}).

The second index used was the relative volumetric error (Pbias), which represents the percent volume difference between simulated and observed streamflow fluxes. Negative Pbias values correspond to model under-estimation and positive ones correspond to over-estimation. The index was calculated using Eq. 14.

$$Pbias(\%) = 1 - \frac{\sum_{k=1}^{Pa}(Q_{TS}(k) - Q_{obs}(k))}{\sum_{k=1}^{Pa} Q_{obs}(k)} * 100 \quad (14)$$

The benefit that can be achieved in streamflow simulation through DA was also measured in this study by means of two additional specific efficiency measures: Eff_{Val} *and* Eff_{OL}, as in Aubert et al. (2003). Eff_{Val} quantifies the improvement (or the deterioration) obtained after (Q_{DA}) compared to the deterministic model validation run (Q_{Val}) (Aubert et al., 2003; Brocca et al., 2010b), and is calculated as in Eq. 15.

$$Eff_{Val} = \left(1 - \frac{\sum_{k=1}^{Pa}(Q_{DA}(k) - Q_{obs}(k))^2}{\sum_{k=1}^{Pa}(Q_{Val}(k) - Q_{obs}(k))^2}\right) * 100 \quad (15)$$

Similarly, Eff_{OL} (Eq. 16) measures the positive or negative effect of DA with respect to the Open-Loop run (Q_{OL}) (Lievens et al., 2015; Cenci et al., 2016), where Q_{OL} is the mean of the ensemble members when no assimilation correction is performed.

$$Eff_{OL} = \left(1 - \frac{\sum_{k=1}^{Pa}(Q_{DA}(k) - Q_{obs}(k))^2}{\sum_{k=1}^{Pa}(Q_{OL}(k) - Q_{obs}(k))^2}\right) * 100 \quad (16)$$

In both Eff_{Val} and Eff_{OL}, positive values denote improvements due to DA, while negative values indicate estimate worsening (Brocca et al., 2010).

Finally, the normalized RMSE (NRMSE) was calculated for a more detailed evaluation of the influence of DA on streamflow simulation. Similarly to Eff_{OL}, this index compares the efficiency after DA with that of the open-loop simulations, and it is calculated as in Eq. 17.

$$NRMSE = \frac{\frac{1}{N_r}\sum_{i=1}^{N_r}\sqrt{\frac{1}{P_a}\sum_{k=1}^{P_a}\left(Q_{DA,i}(k)-Q_{obs}(k)\right)^2}}{\frac{1}{N_r}\sum_{i=1}^{N_r}\sqrt{\frac{1}{P_a}\sum_{k=1}^{P_a}\left(Q_{OL,i}(k)-Q_{obs(k)}\right)^2}} \quad (17)$$

Alvarez-Garreton et al. (2015) recommended NRMSE as it provides information about both the spread of the ensemble and the performance of the ensemble mean. Furthermore, it gives more weight to high flows, since it is calculated in linear streamflow space. NRMSE values below 1 indicate improvements due to DA.

4. Results

4.1. Deterministic model calibration and validation

Fig. 4 displays the results obtained with the two models for the calibration and validation periods, and for Arga and Nestore catchments. It can be observed that although both models adequately predicted the highest streamflow peaks observed in Nestore, a systematic underestimation was found for Arga. This was by some means unexpected, since the same objective function (NSE) was used for the calibration of both models in the two catchments. NSE is suited to fit high peak flows, thus a similar level of accuracy in high flows prediction was expected. The streamflow variability both in the calibration and in the validation periods in Nestore is similar, whereas in Arga, the variability is significantly higher in the calibration than in the validation period (Fig. 4), with all the streamflow peaks below 400 $m^3 s^{-1}$ in the validation and up to 600 $m^3 s^{-1}$ in the calibration period. Almost no large flood events occurred in Arga during the validation period, except for one recorded at the very beginning of this period (Jan 2010).

Figure. 4.

MISDc outperformed TOPLATS in both catchments (Table 1). Additionally, better results were obtained in Nestore than in Arga for both models, in terms of NSE. On the contrary, Pbias errors were very low in Arga compared with Nestore (Table 1). The overall NSE obtained for the whole period studied (including both calibration and validation) was 0.88 and 0.70 for Nestore and 0.75 and 0.64 for Arga, using MISDc and TOPLATS respectively.

Table 1. NSE and Pbias results for the calibration and validation periods obtained using MISDc and TOPLATS models in Nestore and Arga catchments.

Model	Nestore				Arga			
	Cal		Val		Cal		Val	
	NSE	Pbias	NSE	Pbias	NSE	Pbias	NSE	Pbias
MISDc	0.87	-27%	0.90	-6%	0.76	-2%	0.72	0%
TOPLATS	0.70	5%	0.71	38%	0.64	6%	0.58	4%

4.2. ASCAT−SSM preprocessing

- **Soil water index (SWI)**

The optimal *T* values varied from case to case and were higher for Nestore than for Arga, and higher for MISDc than for TOPLATS. For Nestore, optimal values were *T* = 114 days using MISDc (R = 0.88) and *T* = 45 days using TOPLATS (R = 0.65). For Arga, an optimal value of *T* = 64 days was obtained for MISDc (R = 0.90) and a smaller value *T* = 24 days for TOPLATS (R = 0.76). In all cases, correlation (R) values decreased when lower *T* values were tested (results not shown). This decrease of R value was pronounced and very clear in all cases when *T* values approached one. The only exception was Arga with TOPLATS, where the decrease in R for lower *T* values was not that pronounced. SWI calculated for TOPLATS exhibited a larger variability (not shown here), which is related to the shallower soil surface layer considered in this model. In MISDc, the soil layer was deeper, resulting in a smoother SWI temporal dynamic.

- **SWI re-scaling**

Different re-scaling techniques (CDF, LR and VM) lead to different amounts of variability in the resulting time series (Fig. 5 and Fig. 6). SWI time-series obtained through LR and VM methods were very similar, but CDF performed, to some extent, differently. These differences are apparent in the highest and lowest SWI values reached by CDF (e.g., SWI peaks in Fig. 5e, 5g, 6e and 6g). LR was the technique that showed the lowest seasonal dynamics in SWI, with smaller differences between summer and winter values (Fig. 5). Again, TOPLATS simulations had a higher short-term variability than those of MISDc because of its shallower SZ soil layer (Fig.3).

Figure. 5

Figure. 6

4.3. Ensemble validation

Fig. 7 shows the streamflow and SSM ensembles generated by using MISDc (Fig. 7a and 7b) and TOPLATS (Fig. 7c and 7d). It is observed that the SSM ensemble has a larger spread in Nestore (Fig. 7a) than in Arga (Fig. 7b) for the MISDc simulations. Moreover, the ensemble spread appears to be mostly controlled by rainfall perturbation in the TOPLATS ensembles (Fig. 7c and 7d).

The streamflow ensembles successfully met the two validation criteria. Specifically, using MISDc Eq. 11 yielded values of 1.15 for Nestore and 1.1 for Arga, whereas Eq. 12 yielded values of 0.73 for Nestore and 0.72 for Arga; being these sufficiently close to their reference values. TOPLATS also met the required values for Eq. 11: 0.98 for Nestore and 1.01 for Arga; as well as for Eq. 12: 0.71 for Nestore and 0.61 for Arga.

The ensemble spread varied significantly from one model to the other. MISDc had its largest uncertainty during transition and dry periods (Fig. 7a and 7b), while in TOPLATS highest uncertainty rates were found during humid periods (Fig. 7c and 7d). The different perturbation intensities required

to meet the ensemble validation criteria might explain these differences, i.e. for MISDc a stronger parameter perturbation was required, whereas for TOPLATS the two criteria were met when rainfall perturbation magnitude was higher. We are aware that the approach followed in this research to generate the ensembles might not be optimal and subjected to equifinality issues. The methodology used allows satisfying the validation criteria, but for that larger perturbations needed to be applied to parameters with MISDc and to rainfall with TOPLATS. Further research should be devoted to this issue, but in any case, we think that the methodology followed is robust and validates the subsequent application of the ensemble Kalman filter.

Figure. 7.

4.4. SSM-DA in MISDc

In Nestore, the NSE achieved using MISDc in the OL run (0.91) (Table 2) was slightly higher than that of the validation run (0.90) (Fig. 8a). Similarly, in Arga NSE increased from 0.72 in the validation run to 0.73 in the OL run (Fig. 8b). The NSE value of 0.91, achieved in the OL run in Nestore, was not further improved after DA (Fig. 8a), regardless of the different observation error values assumed for the ASCAT data. Furthermore, when low observation errors were considered, NSE decreased sharply, and the other scores also worsened (Fig. 8c, e and g), especially with observation errors below 2 %. Regarding re-scaling methods, CDF produced the worst results, while LR and VM yielded very similar results.

On the other hand, in Arga, DA provided a streamflow simulation improvement (Fig. 8b) when compared to the NSE value (0.73) obtained in the OL run (Table 2). In this catchment, the best NSE improvement was always reached when a 4 % observation error was considered (Table 2), regardless of the applied RT. In this case, the influence of the RTs was only marginal and an increase of 10 % in Eff_{OL} was obtained for all cases (Fig. 8f). It must be noted that assuming satellite observation errors below 1 % led to a significant deterioration in streamflow simulations (NRMSE values above 0 in Fig. 8h).

Fig. 9 shows the MISDc SSM-DA results obtained with the best combination of RT and observation error for Nestore (Fig. 9a) and Arga (Fig. 9b), as detailed in Table 2. Although no improvement was achieved through DA for Nestore, the best combination was considered to be a 1 % observation error and LR re-scaling (Fig. 9a) (Table 2). In Arga (Fig. 9b), the best combination was obtained by using LR re-scaling and a 4 % observation error. DA offered an increase in NSE from 0.72 to 0.76 in this case (Fig 8b). It can be observed that the largest and more systematic improvements were obtained during the spring months of 2010 and 2012 (Fig. 9b, error reduction plot (iii)). On the contrary, DA could not reduce sufficiently the large simulation error (>100 $m^3 s^{-1}$) that MISDc provided on a large event occurred at the beginning of the validation period (Jan 2010) (Fig 9b, plot ii).

Figure. 8.

4.5. SSM-DA in TOPLATS

A high NSE result (0.71) was already obtained after validating TOPLATS in Nestore. In this case, a significant improvement was already obtained in the OL run, increasing NSE to 0.77 (Fig. 8i) (Table 2). This value further increased after SSM−DA to a value of 0.85 (Fig. 8i). SSM-DA also reduced the large Pbias value obtained for Nestore during validation to a value of approximately 20 % when LR re-scaling was used (Fig. 8k) and led to improved Eff_{OL} values of 34 % (Fig. 8m).

The improvements for Arga were not that remarkable, with a total NSE increase from 0.58 during validation (and 0.60 for OL) to 0.62 after SSM−DA when a 6 % observation error was considered (Fig. 8j) (Table 2). Using this error value, there was a slight reduction in the Pbias value to 9 % (Fig. 8l), and the efficiency increase (Eff_{OL}) was 6 % (Fig. 8n).

Clear differences in terms of NSE variation were found depending on the RT applied (Fig. 8i and 8j), with LR providing the best results, followed by VM for Nestore and CDF for Arga. For Nestore, any combination of RT and observation error increased Eff_{OL} by at least 8 % (Fig. 8m). In fact, this was the case where DA provided the highest improvements out of the four combinations of models and catchments evaluated. On the other hand, the DA results for Arga depended strongly on the

observation error considered. When observation errors below 4 % were used and CDF or VM re-scaling was applied, the efficiency was lower than in the OL run (Fig. 8n). The highest efficiencies, regardless of RT applied, were obtained for Arga with observation errors within the 4-8 % range, while the best improvements for Nestore were obtained by considering low (<2 %) observation errors.

In Nestore, the largest errors in the simulation were found during two important events (that reached up to 400 m^3/s observed streamflow peaks), one in Jan 2010 and the other in Nov 2010 (Fig. 9c, plot i); these were not accurately simulated, with errors over 100 m^3/s (Fig. 9c, plot ii). These large errors were substantially reduced after DA (using LR and a 0.01 % observation error (Table 2)), with a correction of up to 100 m^3/s for the first event and over 50 m^3/s for the second (Fig. 9c, plot iii). In Arga (Fig. 9d), the largest error was also found for a storm event that occurred at the beginning of the validation period (Jan 2010). However, DA did not succeed in reducing this error (it was even increased during certain times of the event). More substantial improvements were obtained in 2011 and 2012 during spring months (Fig 9d, plot iii).

Table 2. Summary of results and efficiency variations after best set-up DA application. Optimal rescaling method (Opt. RT) and ASCAT observation error (Opt. ASCAT) are also shown.

Model	Catchment	Cal/val	Cal/Val	OL	Opt. ASCAT observation Error	Opt. RT	DA			
		Cal	Val	Val			Val			
		NSE	NSE	NSE			NSE	Eff_{Val}	Eff_{OL}	NRMSE
MISDc	Nestore	0.87	0.90	0.91	1%	LR	0.90	-20 %	-13 %	1.06
	Arga	0.76	0.72	0.73	4%	LR	0.76	10 %	10 %	0.95
TOPLATS	Nestore	0.70	0.71	0.77	<1%	LR	0.85	48 %	34 %	0.81
	Arga	0.64	0.58	0.60	6%	LR	0.62	10 %	6%	0.97

Figure. 9.

4.6. Comparison of SSM-DA results for the MISDc and TOPLATS models

As a summary of results and to provide a numerical and visual comparison of SSM-DA performance for both models, the Eff_{Val} index was used (Fig. 10). Best Eff_{Val} results and SSM-DA set-up for obtaining them are also shown in Table 2.

Figure. 10.

In the first case, i.e., using MISDc for Nestore, SSM−DA did not provide any streamflow simulation improvement, regardless of the RT used and the SSM observation error assumed (Fig. 10a). On the contrary, large Eff_{Val} improvements (>30 %) were obtained for this catchment using TOPLATS (Fig. 10c), irrespective of the observation error or the RT. In Nestore, both models yielded the best results when LR re-scaling was used. With respect to Arga, the DA improvements were similar for both models (Fig. 10b and d). SSM-DA improved Eff_{Val} by a 10 %, especially when observation errors between 4 % and 8 % were considered. Lower observation errors resulted in a worsening of model forecasts. The differences among the selected RTs were smaller for Arga than for Nestore, but in all cases, LR was the best method.

4.7. Monthly evaluation

Figure. 11.

In Nestore, SSM-DA generally decreased MISDc model accuracy in terms of monthly simulation (Fig. 11a). On the contrary, the error reduction thanks to SSM-DA was high for this catchment when TOPLATS was used (Fig. 11c), especially in the winter months (from November until March). This seasonal trend contrasted with that obtained for Arga using TOPLATS (Fig. 11d), where the largest corrections were observed in November and later in spring (April and May). On the contrary, no clear seasonal pattern was found for the MISDc DA results for Arga (Fig. 11b), where most of the

improvement occurred in May and June. Interestingly, for Arga, highest correction rates after DA were achieved in May and November (i.e. transition humid-dry periods) for both models.

5. Discussion

Despite significant efforts in SSM-DA research, there is still no consensus in the scientific community regarding the improvement in streamflow prediction skill to be expected after SSM-DA because many factors affect the DA performance. These factors include: the DA algorithm, the particular model structure, the choice of bias correction technique, the appropriate quantification of observation and model forecast errors, the spatial mismatching between modelled and satellite soil moisture, and the watershed topography and climatology (Yan and Moradkhani, 2016). Through the use of different models, RTs, observation errors, and catchments, this research aimed to develop a broad study that could provide valuable results regarding some of these factors. The results are discussed based on the following research questions:

1) Did EnKF SSM-DA improve hourly streamflow prediction?

This study demonstrated that ASCAT-derived SWI can improve hourly streamflow simulation of medium-sized (750 km^2) Mediterranean catchments using physically based and conceptual models. Moreover, a significant specific merit of this study is that the improvements were achieved in a fully independent validation period, different to the periods used for model calibration and SWI RTs calibration. As shown in Figures 8, 10 and 11, in one of the models (TOPLATS), DA improved streamflow prediction for Nestore, while in both models DA improved the Arga simulations. The results obtained for Arga using MISDc are of similar magnitude as those reported in the literature, such as Brocca et al. (2010b), who reported NSE increases from 0.76 to 0.78 and from 0.60 to 0.63 in catchments of central Italy after ASCAT SSM-DA. Also with respect to MISDc model application, similar results were obtained by Brocca et al. (2012), where ASCAT SSM-DA improved NSE from 0.76 to 0.79 and increased $Eff_{Val} \approx 10$ %, but in smaller Mediterranean catchments. Regarding TOPLATS DA results, the efficiency improvements after ASCAT−SSM assimilation outperformed

those of previous TOPLATS-DA studies (Pauwels et al., 2002, 2001), which in any case already indicated that this model was suitable for improvements in simulation capability through DA. Similarly, different SSM-DA methods were tested using TOPLATS by Houser et al. (1998) whose resulting recommendations included the use of DA methods of moderate complexity that are sound and computationally efficient, and recommended the use of long data series, as it has been done in this study. Although the DA method used might have a significant effect on the assimilation results (Yan and Moradkhani, 2016), this was not the focus of this research.

The variability of the results in our study is not exceptional in the SSM−DA literature. Studies of this type have reported a variety of results, ranging from successful improvements (Lievens et al., 2015; López López et al., 2016), to slight improvements (Pauwels et al., 2002), no significant differences (Lü et al., 2016) or even moderate decreases in model performance (Chen et al., 2011; Matgen et al., 2012a). Studies on the topic cover a wide range of catchment sizes, climate conditions, remote sensing sources, model conceptualizations and assimilation methods. Among the studies where SSM−DA proved ineffective in improving streamflow forecasts (e.g., Chen et al. (2011), Draper et al. (2011), Han et al. (2012)), some authors noted that the limited efficiency of DA might be related to the inaccuracy of the rainfall-runoff simulation mechanism in the models (Han et al., 2012). Also, other studies reported that while dual assimilation of streamflow and ASCAT−SSM improved streamflow simulation, SSM assimilation alone did not result in any improvements (Yan and Moradkhani, 2016).

On the other hand, other studies obtained more positive results and confirmed the possibility of enhancing model streamflow prediction through remotely sensed SSM−DA (Alvarez-Garreton et al., 2014; Massari et al., 2015; Matgen et al., 2012b). Improvements were reported using different metrics: efficiency increases between ~10 % (Matgen et al., 2012b) and ~30 % (Massari et al., 2015) and NRMSE reductions of ~25 % (Alvarez-Garreton et al., 2014) were obtained. Laiolo et al. (2015a) also reported an $Eff_{OL} \approx 25$ to 35 %, for ASCAT SSM-DA in an Italian catchment of 800 km^2. ASCAT−SSM assimilation based on the EnKF also improved streamflow forecasts for larger

catchments (Wanders et al., 2014b), although some limitations to simulate high peaks flow were found.

Lastly, in relation to the results obtained by the OL, it was found that although no improvements were obtained with MISDc, some improvements were obtained with TOPLATS, especially in Nestore (Figure 8i). In our opinion this is related to the models structure, specifically to the non-linearities in runoff generation within TOPLATS. Adding uncertainty to the model inputs, i.e., moving from a deterministic approach (of streamflow simulation) to a stochastic one could reduce this non-linearities and provide efficiency increases.

Did monthly simulation improve after EnKF data assimilation?

As shown in Fig. 11, the DA impacts differed depending on the season and on the particular model and catchment combination, with no clear or consistent patterns. In Arga (Fig. 11b and 11d), ASCAT−SSM assimilation improved both models' performance, especially in the autumn and spring months (mainly in Nov and May). These results are in line with those of Cenci et al. (2016), Laiolo et al. (2015b) and Matgen et al. (2012a), who showed that ASCAT−SSM assimilation was more efficient during hydro-meteorological transition periods (e.g., from dry to wet seasons or vice versa). In these periods, the temporal variability of SSM is generally higher, and its correction might have a stronger impact on model performance (Massari et al., 2015). On the contrary, in Nestore the largest positive results were obtained during winter months with the TOPLATS model (Fig. 11c), as in Laiolo et al. (2015a).

2) Did the SWI calculation and the re-scaling techniques have a significant influence on the DA results?

Normally, *T* is expected to increase with the depth of the modeled layer, but it has also been related to different catchment characteristics, such as soil type, land use or climatic conditions (Wang et al., 2017). In this study, the *T* values obtained for TOPLATS are to some extent higher than the ones found in the literature for layers of this depth (Alvarez-Garreton et al., 2015). Previous works on the

topic found that large *T* values can be problematic for assimilation, since they might lead to SWI series with autocorrelation structures different from the modeled ones (Qiu et al., 2014). In relation to this issue, Qiu et al. (2014) performed a series of synthetic analysis where the impact of this autocorrelation mismatch on SSM-DA was quantified. They found that the benefit of DA was compromised in cases where differences persisted, but also concluded that DA performance deteriorated specially for deeper soil layers and in cases where the vertical redistribution of the soil water was relatively slow, which was not the case in our study with TOPLATS, where water transfers quickly from the SZ layer into the deeper TZ layer, and SSM data is assimilated into a shallow 5 cm depth layer.

In addition to the results shown in this paper, two supplementary SSM-DA experiments were performed (not shown) by selecting lower *T* values for the SWI calculation with TOPLATS model. The results obtained showed only slightly decreasing efficiencies, indicating that the influence of the *T* value applied might be not be as noteworthy as it could be initially expected. In our view, further detailed studies are required in this topic to fully understand the complex SM behaviors represented by parameter *T*.

All in all, there is still no clear consensus on the optimal *T* value ranges, and on the effect that the simulated layer depth, soil type or land use has on these optimal values. Moreover, as indicated in Wang et al. (2017), forested areas, which occupy large areas in the studied catchments, are expected to cause higher *T* values than other land uses. While in general this is a topic that needs further understanding and research, we think that model structure, especially the number and depth of the layers configured within each model used to calculate the SWI needs to be analyzed to evaluate whether it has influence on the *T* obtained. In this sense, we believe that the high optimal *T* values obtained in this study are probably partly related to the quick transfer that occurs downwards from SZ to TZ. Thus, DA in TOPLATS corrects first the SSM in the SZ, but these corrections are quickly transferred to the deeper TZ and thus varying the water table depth, which could indicate that the

achieved large *T* values tend to represent the SM behavior within the whole modeled system, and that SM behavior in the upper layer should not be independently evaluated.

Regarding the impact of RTs in DA results, the results obtained here do not fully agree with those reported by Massari et al. (2015), who observed only a small effect of re-scaling on assimilation results. Although all three RTs behaved similarly in some cases (MISDc used in Arga) (Fig. 8h), large differences were found in other cases (e.g., TOPLATS used in Nestore (Fig. 8o)). In any case, LR consistently produced the best results and CDF the poorest. Lievens et al. (2015) found that a first-order matching (similar to the LR-RT applied here) provided better results than higher-order CDF matching techniques. Yilmaz and Crow (2013) also discussed the risks associated with applications of RT methods that match the total variance of observations with the model (VM and CDF), as they may partly neglect the noise contributions of the datasets.

According to the results in our study, it could be inferred that VM and CDF seem to fit "too much" the observed data to the simulated data, thus leaving only a minimal influence for DA that, at least on the model/catchment conditions evaluated in this study, offered the poorest results. It seems that other methods, such as LR – that offer more degree of freedom to the observations – perform a more truthful correction through DA. Moreover, simulated SSM might have seasonal specific behaviors, which can affect RTs performance for DA. This could be specifically significant for CDF method, as it is the one performing a more intense fitting of the observations. Separate seasonal re-scaling calibrations should thus be explored in future works to evaluate this influence.

3) Did the observation error have a significant influence on the SSM-DA results?

The estimation of an appropriate observation error for DA techniques is a key question that is still open and requires further research (Trudel et al., 2014; Massari et al., 2015). Different studies have attempted to characterize the satellite SSM error either by comparing satellite SSM data with ground observations (Albergel et al., 2009; Brocca et al., 2010; Matgen et al., 2012b) or by providing an independent error estimate. For instance, since a DA scheme explicitly updates the model prediction

based on the relative weights of the model and the observation errors, assuming a constant observation error may lead to overcorrection of the model state if the actual error is higher, and vice versa. To this end, a valuable approach for observation error selection is the application of the TC technique, which has shown to provide reliable results (Dorigo et al., 2010, 2015; Chen et al., 2014; Renzullo et al., 2014; Su and Ryu, 2015; Alvarez-Garreton et al., 2016) and would need further explorations. Furthermore, data providers also supply quality indexes as ancillary data which can be extremely useful for a first assessment of the quality of the satellite observations (Kerr et al., 2010). Nonetheless these indexes do not provide a quantitative estimate of the random error associated with the SSM observations and are difficult to use within any DA scheme. A possible solution is the calibration of the observation error which is the route taken in this study.

The optimal values for the observation errors obtained here are lower than the 10% value shown by Albergel et al. (2009), Brocca et al. (2010) and Matgen et al. (2012b) for ASCAT; but error estimations in this study refer to the SWI transformed data so they are not fully comparable with those reported in literature. Our results reveal that the characteristics of the site can influence the optimal observation error value to be used within SSM-DA, but also the model used. Altogether, the observation error estimated for the ASCAT SSM product had a clear influence on the assimilation results and it must be selected with care. That influence is especially critical when error values below 2% are applied (e.g. Fig 8a and 8b, where a sharp decrease on the efficiency occurred when observation error values below 2% were applied). On the contrary, varying observation error values within the 10 to 20% range, does not generate large efficiency variations (Fig 8a, 8b, 8i and 8j). Moreover, the applied observation error had a greater influence in MISDc than in TOPLATS model experiments.

4) Did the model choice influence the results?

The differences found in the results might not be explained by the type of model but rather by the accuracy of model predictions before SSM-DA (i.e., after calibration). Antecedent works already indicated that the increase in the performance after the SSM–DA was dependent on the quality of the

simulation achieved in the OL (Alvarez-Garreton et al., 2015, Matgen et al., 2012a); this effect is clearly visible in the results obtained here using MISDc in Nestore, where an NSE of 0.90 during the validation period offered few possibilities for further improvements through SSM–DA. In this sense, some studies have used SSM–DA as a tool for improving model parameter calibration instead of directly enhancing streamflow simulation (Bach and Mauser, 2003; Moradkhani et al., 2005; Wanders et al., 2014a).

In this study, it was found that the added value of SSM–DA varied strongly in the four different model-catchment settings evaluated here. For Arga, regardless of the model applied (MISDc or TOPLATS), we obtained similar simulation improvements of ~10 % (Fig 10b and 10d). On the other hand, the results obtained for Nestore varied dramatically depending on the model used, with improvements of ~50 % using TOPLATS but a worsening effect of >50 % for MISDc (Fig 10a and 10c). Therefore, it cannot be concluded that model type and its complexity influences DA results in a specific positive or negative direction. Moreover, this study also found that the assimilation of SSM data into a thin surface layer of a model (TOPLATS) does not limit the capabilities of DA to substantially vary streamflow simulations, in contrast to Brocca et al. (2012).

Differences in ensemble spread (highly related to the different parameters perturbed in each model) are also expected to affect the susceptibility of each model to be corrected through DA. As shown in Figure 7, and discussed in section 4.3, MISDc showed larger uncertainty rates (spread) on its prediction during transition and dry periods, while TOPLATS showed to be less precise during winter seasons. These ensemble spreads would indicate a higher ease to be corrected during summer storms in MISDc, and in softer and longer winter events in TOPLATS. But, in any case, as described in the previous paragraphs, the results were much more conditioned by the efficiency after calibration and by the catchment characteristics (discussed in the next question), rather than by the model used.

5) Was DA performance influenced by catchment characteristics?

Soil type and catchment characteristics, unlike catchment area, might play a role in the performance of SSM-DA (Massari et al., 2015). The significant improvement in NSE obtained for Nestore using TOPLATS can be explained by the climate conditions of the area. Since central Italy is not characterized by a proper rainy season, soil hardly remains constantly saturated. Under such conditions, when a significant meteorological event occurs, SM conditions change rapidly. Therefore, SSM−DA might be useful for correcting the antecedent wetness conditions, thus contributing to an enhanced prediction of high flows (Cenci et al., 2016). SSM−DA might be more efficient when SSM temporal variability is higher (Massari et al. 2015) and direct runoff processes are predominant (instead of baseflow contribution) (López López et al., 2016). In any case, as pointed out in the monthly results analysis section, it must be noted that most of the improvement in Nestore is concentrated on winter months events. On the other hand, longer and more stable dry and wet climatic patterns, characteristic of the Arga catchment, somehow limited the effectivity of DA in this catchment to certain particular transition periods (e.g., November and May) where model inertia did not enable a rapid response of the model to generate the correct simulated runoff.

6) Which topics within SSM DA require further research and better understanding for improved streamflow prediction?

As a complement to the assimilation approach used in this study (assimilation of SSM observations into the upper soil layer), we would recommend further experiments to explore the assimilation of SSM observations into TOPLATS Transmission Zone (deeper layer), and the use of DA to correct the water table behavior, which is crucial for the runoff processes of this model. In addition to this, there are three different issues that would also require further research: (1) a thorough evaluation of the added value of SSM−DA compared to the enhancements achieved when other variables (e.g., streamflow or LAI) are assimilated, (2) the identification of the causes of model bias as a means of enhancing simulations depending on the particular cause (i.e., poor model calibration, errors in forcing data, model structure, etc.), rather than relying on DA as a tool for fixing everything, and (3) the development of models that better reflect the vertical coupling between surface and subsurface soil moisture states. As shown in this work, there is potential to improve catchment model streamflow

simulations through data assimilation of remotely sensed soil moisture products. However, systematic model bias must first be reduced to a minimum, through calibration, so as to not constrain soil moisture data assimilation capabilities.

6. Conclusions

This study has demonstrated that ASCAT-derived soil water index assimilation into models with different conceptualization approaches can improve hourly streamflow simulation in medium-size catchments located in Mediterranean climate areas when an adequate DA configuration, in terms of surface soil moisture observation re-scaling and observation error, is set-up. The main findings are summarized as follows:

After model calibration, streamflow forecasts were more accurate using a conceptual and less parameterized model (i.e., MISDc) than with a physically based complex one (TOPLATS). In any case, both models offered overall Nash-Sutcliffe efficiencies (NSE) > 0.65 for the 11 years studied period. ASCAT data assimilation increased the Nash-Sutcliffe efficiency in three out of four catchment/hydrological model combinations evaluated. For the remaining case, DA could not increase model performance due to the already high NSE efficiency.

The open-loop ensemble streamflow simulation (Q_{OL}) outperformed the deterministic simple model validation (VAL) run in both models. Whereas the increase was minor in MISDc, in TOPLATS moderate (Arga) and large (Nestore) improvements were obtained. Thus, this study indicates that considering forcing and parameter uncertainties in modelization with models that include non-linear processes, could lead to improvements in streamflow simulation efficiencies, while providing more robust results, and offering information about the confidence interval of the achieved results. In this line, further studies are required to fully understand the impact of uncertainty addition on model performance.

The re-scaling technique used strongly conditioned the results obtained, with linear re-scaling (LR) offering better results than variance matching (VM) and cumulative distribution function matching (CDF), especially with TOPLATS. Besides, the ASCAT surface soil moisture observation error largely influenced the assimilation results, with the best SSM-DA performance achieved when low observation error values (4-6 %, or even <1 %) were considered.

It was difficult to extract very conclusive ideas on the influence of model structure on DA, due to the large number of processes involved on the assimilation set-up, and due to the complex interactions between them. In this study results, the magnitude of the DA impact seemed to be more related to the specific catchment conditions rather than to a specific model characteristic (i.e. conceptualization and parameterization complexity or soil layer configuration). Impact of DA, in terms of its magnitude (both positive and negative), were larger in Nestore catchment (>50% from the validation run) than in Arga (≈10% from the validation run) regardless of the model used. In addition to this, the success achieved in model calibration for a specific catchment had a great influence on the ability of DA to improve its predictions.

In summary, SSM-DA, through the ensemble Kalman filter, provided efficiency increases that reached 10-45% from the validation run and 6-35% from the open-loop simulation, with this variation depending largely on: the catchment characteristics, the assumed SSM observation error, and the selected re-scaling technique.

The re-scaling techniques were calibrated and validated for separate periods, which makes this study consistent in terms of avoiding data correlation issues and inadequate fitting of the data. However, this study should not be considered as a perfectly controlled sensitivity analysis of the different assimilation set-up scenarios for every catchment and model used for DA. Achieving a better understanding of the DA scheme sensitivity and of the underlying physical and methodological meaning of this sensitivity would require more systematical experiments. Nevertheless, we think that this research was able to identify several recommendations for further SSM-DA applications: 1) each

catchment/model/SSM product configuration should go through a "calibration" process to find their optimal experimental setup, 2) if only one re-scaling technique is to be used, LR should be recommended, and 3) observation error calibration efforts should focus on the 1-6% range. In relation to the estimation of the observation error, further studies that evaluate the relation between land-use information and applied observation error should be of interest.

Acknowledgements

This study was partially funded by the Spanish Ministry of Science and Innovation (Project CGL2011-24336), the Spanish Ministry of Innovation and Competitiveness (Project CGL2015-64284-C2-1-R MINECO/FEDER) and by the Public University of Navarre through a pre-doctorate research scholarship to the first author.

References

Abaza, M., Anctil, F., Fortin, V., Turcotte, R., 2015. Exploration of sequential streamflow assimilation in snow dominated watersheds. Adv. Water Resour. 86, 414–424. doi:10.1016/j.advwatres.2015.10.008

Albergel, C., de Rosnay, P., Gruhier, C., Muñoz-Sabater, J., Hasenauer, S., Isaksen, L., Kerr, Y., Wagner, W., 2012. Evaluation of remotely sensed and modelled soil moisture products using global ground-based in situ observations. Remote Sens. Environ. 118, 215–226. doi:10.1016/j.rse.2011.11.017

Albergel, C., Rüdiger, C., Carrer, D., Calvet, J.C., Fritz, N., Naeimi, V., Bartalis, Z., Hasenauer, S., 2009. An evaluation of ASCAT surface soil moisture products with in-situ observations in Southwestern France. Hydrol. Earth Syst. Sci. 13, 115–124.

Albergel, C., Rüdiger, C., Pellarin, T., Calvet, J.C., Fritz, N., Froissard, F., Suquia, D., Petitpa, A., Piguet, B., Martin, E., 2008. From near-surface to root-zone soil moisture using an exponential filter: An assessment of the method based on in-situ observations and model simulations. Hydrol. Earth Syst. Sci. 12, 1323–1337.

Alvarez-Garreton, C., Ryu, D., Western, A.W., 2013. Impact of observation error structure on satellite soil moisture assimilation into a rainfall-runoff model. 20th Int. Congr. Model. Simul.

Alvarez-Garreton, C., Ryu, D., Western, A.W., Crow, W.T., Robertson, D.E., 2014. The impacts of assimilating satellite soil moisture into a rainfall-runoff model in a semi-arid catchment. J. Hydrol.

Alvarez-Garreton, C., Ryu, D., Western, A.W., Crow, W.T., Su, C.H., Robertson, D.R., 2016. Dual assimilation of satellite soil moisture to improve streamflow prediction in data-scarce catchments. Water Resour. Res. 52, 5357–5375. doi:10.1002/2015WR018429

Alvarez-Garreton, C., Ryu, D., Western, A.W., Su, C.-H., Crow, W.T., Robertson, D.E., Leahy, C., 2015. Improving operational flood ensemble prediction by the assimilation of satellite soil moisture: comparison between lumped and semi-distributed schemes. Hydrol. Earth Syst. Sci. 19, 1659–1676. doi:10.5194/hess-19-1659-2015

Attema, E.P.W., Ulaby, F.T., 1978. Vegetation modeled as a water cloud. Radio Sci. 13. doi:10.1029/RS013i002p00357

Aubert, D., Loumagne, C., Oudin, L., 2003. Sequential assimilation of soil moisture and streamflow data in a conceptual rainfall - Runoff model. J. Hydrol. 280, 145–161.

Bach, H., Mauser, W., 2003. Methods and examples for remote sensing data assimilation in land surface process modeling. IEEE Trans. Geosci. Remote Sens. 41, 1629–1637. doi:10.1109/TGRS.2003.813270

Bartalis, Z., Wagner, W., Naeimi, V., Hasenauer, S., Scipal, K., Bonekamp, H., Figa, J., Anderson, C., 2007. Initial soil moisture retrievals from the METOP-A Advanced Scatterometer (ASCAT). Geophys. Res. Lett. 34.

Beven, K.J., Kirkby, M.J., 1979. Physically based, variable contributing area model of basin hydrology. Hydrol Sci Bull Sci Hydrol 24, 43–69.

Bhimala, K.R., Goswami, P., 2015. A Comparison of ASCAT Soil Moisture Data With In Situ Observations Over the Indian Region: A Multiscale Analysis. IEEE Trans. Geosci. Remote Sens. 53. doi:10.1109/TGRS.2015.2422377

Blaney, H.F., Criddle, W.D., 1950. Determining Water Requirements in Irrigated Areas from Climatological and Irrigation Data. USDA, SCS-TP-96.

Brocca, L., Hasenauer, S., Lacava, T., Melone, F., Moramarco, T., Wagner, W., Dorigo, W., Matgen, P., Martínez-Fernández, J., Llorens, P., Latron, J., Martin, C., Bittelli, M., 2011a. Soil moisture estimation through ASCAT and AMSR-E sensors: An intercomparison and validation study across Europe. Remote Sens. Environ. 115, 3390–3408.

Brocca, L., Liersch, S., Melone, F., Moramarco, T., Volk, M., 2013. Application of a model-based rainfall-runoff database as efficient tool for flood risk management. Hydrol. Earth Syst. Sci. 17, 3159–3169.

Brocca, L., Melone, F., Moramarco, T., 2011b. Distributed rainfall-runoff modelling for flood frequency estimation and flood forecasting. Hydrol. Process. 25, 2801–2813.

Brocca, L., Melone, F., Moramarco, T., 2008. On the estimation of antecedent wetness conditions in rainfall–runoff modelling. Hydrol. Process. 22, 629–642. doi:10.1002/hyp.6629

Brocca, L., Melone, F., Moramarco, T., Morbidelli, R., 2009a. Antecedent wetness conditions based on ERS scatterometer data. J. Hydrol. 364, 73–87.

Brocca, L., Melone, F., Moramarco, T., Singh, V.P., 2009b. Assimilation of observed soil moisture data in storm rainfall-runoff modeling. J. Hydrol. Eng. 14, 153–165.

Brocca, L., Melone, F., Moramarco, T., Wagner, W., Hasenauer, S., 2010a. ASCAT soil wetness index validation through in situ and modeled soil moisture data in central Italy. Remote Sens. Environ. 114, 2745–2755. doi:10.1016/j.rse.2010.06.009

Brocca, L., Melone, F., Moramarco, T., Wagner, W., Naeimi, V., Bartalis, Z., Hasenauer, S., 2010b. Improving runoff prediction through the assimilation of the ASCAT soil moisture product. Hydrol. Earth Syst. Sci. 14, 1881–1893.

Brocca, L., Moramarco, T., Melone, F., Wagner, W., Hasenauer, S., Hahn, S., 2012. Assimilation of surface- and root-zone ASCAT soil moisture products into rainfall-runoff modeling. IEEE Trans. Geosci. Remote Sens. 50, 2542–2555.

Brooks, R.H., Corey, A.T., 1964. Hydraulic properties of porous media and their relation to drainage design. Trans. ASABE 7, 26–0028.

Camici, S., Tarpanelli, A., Brocca, L., Melone, F., Moramarco, T., 2011. Design soil moisture estimation by comparing continuous and storm-based rainfall-runoff modeling. Water Resour. Res. 47, W05527. doi:10.1029/2010WR009298

Cenci, L., Laiolo, P., Gabellani, S., Campo, L., Silvestro, F., Delogu, F., Boni, G., Rudari, R., 2016. Assimilation of H-SAF Soil Moisture Products for Flash Flood Early Warning Systems . Case Study: Mediterranean Catchments. Accept. Publ. IEEE J. Sel. Top. Appl. Earth Obs. Remote Sens. July 2016. doi:10.1109/JSTARS.2016.2598475

Chen, F., Crow, W.T., Ryu, D., 2014. Dual Forcing and State Correction via Soil Moisture Assimilation for Improved Rainfall–Runoff Modeling. J. Hydrometeorol. 15, 1832–1848. doi:10.1175/JHM-D-14-0002.1

Chen, F., Crow, W.T., Starks, P.J., Moriasi, D.N., 2011. Improving hydrologic predictions of a catchment model via assimilation of surface soil moisture. Adv. Water Resour. 34, 526–536. doi:10.1016/j.advwatres.2011.01.011

Chen, F., Crow, W.T., Starks, P.J., Moriasi, D.N., 2011. Improving hydrologic predictions of a catchment model via assimilation of surface soil moisture. Adv. Water Resour. 34, 526–536.

Cho, E., Choi, M., Wagner, W., 2015. An assessment of remotely sensed surface and root zone soil moisture through active and passive sensors in northeast Asia. Remote Sens. Environ. 160, 166–179. doi:10.1016/j.rse.2015.01.013

Crow, W.T., Bindlish, R., Jackson, T.J., 2005. The added value of spaceborne passive microwave soil moisture retrievals for forecasting rainfall-runoff partitioning. Geophys. Res. Lett. 32, 1–5.

Crow, W.T., Drusch, M., Wood, E.F., 2001. An observation system simulation experiment for the impact of land surface heterogeneity on AMSR-E soil moisture retrieval. IEEE Trans. Geosci. Remote Sens. 39, 1622–1631.

Crow, W.T., Reichle, R.H., 2008. Comparison of adaptive filtering techniques for land surface data assimilation. Water Resour. Res. 44, n/a-n/a. doi:10.1029/2008WR006883

Crow, W.T., Ryu, D., 2009. A new data assimilation approach for improving runoff prediction using remotely-sensed soil moisture retrievals. Hydrol. Earth Syst. Sci. 13, 1–16.

Crow, W.T., Van Den Berg, M.J., 2010. An improved approach for estimating observation and model error parameters in soil moisture data assimilation. Water Resour. Res. 46.

Crow, W.T., Wood, E.F., 2003. The assimilation of remotely sensed soil brightness temperature imagery into a land surface model using Ensemble Kalman filtering: A case study based on ESTAR measurements during SGP97. Adv. Water Resour. 26, 137–149.

De Lannoy, G.J.M., Houser, P.R., Pauwels, V.R.N., Verhoest, N.E.C., 2006. Assessment of model uncertainty for soil moisture through ensemble verification. J. Geophys. Res. Atmos. 111.

Demaria, E.M., Nijssen, B., Wagener, T., 2007. Monte Carlo sensitivity analysis of land surface parameters using the Variable Infiltration Capacity model. J. Geophys. Res. 112, D11113. doi:10.1029/2006JD007534

Dickinson, R.E., 1984. Modeling evapotranspiration for three-dimensional global climate models. Clim. Process. Clim. Sensit.

Dorigo, W.A., Gruber, A., De Jeu, R.A.M., Wagner, W., Stacke, T., Loew, A., Albergel, C., Brocca, L., Chung, D., Parinussa, R.M., Kidd, R., 2015. Evaluation of the ESA CCI soil moisture product

using ground-based observations. Remote Sens. Environ. 162, 380–395. doi:10.1016/j.rse.2014.07.023

Dorigo, W.A., Scipal, K., Parinussa, R.M., Liu, Y.Y., Wagner, W., De Jeu, R.A.M., Naeimi, V., 2010. Error characterisation of global active and passive microwave soil moisture datasets. Hydrol. Earth Syst. Sci. 14. doi:10.5194/hess-14-2605-2010

Draper, C., Mahfouf, J.F., Calvet, J.C., Martin, E., Wagner, W., 2011. Assimilation of ASCAT near-surface soil moisture into the SIM hydrological model over France. Hydrol. Earth Syst. Sci. 15, 3829–3841. doi:10.5194/hess-15-3829-2011

Draper, C.S., Reichle, R.H., De Lannoy, G.J.M., Liu, Q., 2012. Assimilation of passive and active microwave soil moisture retrievals. Geophys. Res. Lett. 39. doi:10.1029/2011GL050655

Draper, C.S., Walker, J.P., Steinle, P.J., de Jeu, R.A.M., Holmes, T.R.H., 2009. An evaluation of AMSR-E derived soil moisture over Australia. Remote Sens. Environ. 113. doi:10.1016/j.rse.2008.11.011

Drusch, M., 2005. Observation operators for the direct assimilation of TRMM microwave imager retrieved soil moisture. Geophys. Res. Lett. 32, L15403. doi:10.1029/2005GL023623

Elsanabary, M.H., Gan, T.Y., 2015. Evaluation of climate anomalies impacts on the Upper Blue Nile Basin in Ethiopia using a distributed and a lumped hydrologic model. J. Hydrol. doi:10.1016/j.jhydrol.2015.09.052

Entekhabi, D., Njoku, E.G., O'Neill, P.E., Kellogg, K.H., Crow, W.T., Edelstein, W.N., Entin, J.K., Goodman, S.D., Jackson, T.J., Johnson, J., Kimball, J., Piepmeier, J.R., Koster, R.D., Martin, N., McDonald, K.C., Moghaddam, M., Moran, S., Reichle, R., Shi, J.C., Spencer, M.W., Thurman, S.W., Tsang, L., Van Zyl, J., 2010. The soil moisture active passive (SMAP) mission. Proc. IEEE 98. doi:10.1109/JPROC.2010.2043918

Evensen, G., 2003. The Ensemble Kalman Filter: theoretical formulation and practical implementation. Ocean Dyn. 53, 343–367. doi:10.1007/s10236-003-0036-9

Evensen, G., 1994. Sequential data assimilation with a nonlinear quasi-geostrophic model using Monte Carlo methods to forecast error statistics. J. Geophys. Res. 99, 10,110-143,162.

Famiglietti, J.S., Wood, E.F., 1994. Multiscale modeling of spatially variable water and energy

balance processes. Water Resour. Res. 30, 3061–3078.

Franchini, M., Wendling, J., Obled, C., Todini, E., 1996. Physical interpretation and sensitivity analysis of the TOPMODEL. J. Hydrol. 175, 293–338.

Francois, C., Quesney, A., Ottle, C., 2003. Sequential assimilation of ERS-1 SAR data into a coupled land surface-hydrological model using an extended Kalman filter. J. Hydrometeorol. 4, 473–487. doi:10.1175/1525-7541(2003)4<473:SAOESD>2.0.CO;2

Gordon, N.J., Salmond, D.J., Smith, A.F.M., 1993. Novel approach to nonlinear/non-gaussian Bayesian state estimation. IEE Proceedings, Part F Radar Signal Process. 140, 107–113.

Gupta, V.K., Waymire, E., Wang, C.T., 1980. A representation of an instantaneous unit hydrograph from geomorphology. Water Resour. Res. 16, 855–862. doi:10.1029/WR016i005p00855

Hahn, S., Melzer, T., Wagner, W., 2012. Error assessment of the initial near real-time METOP ASCAT surface soil moisture product. IEEE Trans. Geosci. Remote Sens. 50, 2556–2565. doi:10.1109/TGRS.2012.2183877

Han, E., Merwade, V., Heathman, G.C., 2012. Implementation of surface soil moisture data assimilation with watershed scale distributed hydrological model. J. Hydrol. 416–417, 98–117. doi:10.1016/j.jhydrol.2011.11.039

Han, E., Merwade, V., Heathman, G.C., 2012. Implementation of surface soil moisture data assimilation with watershed scale distributed hydrological model. J. Hydrol. 416–417, 98–117.

Houser, P.R., Shuttleworth, W.J., Famiglietti, J.S., Gupta, H. V, Syed, K.H., Goodrich, D.C., 1998. Integration of soil moisture remote sensing and hydrologic modeling using data assimilation. Water Resour. Res. 34, 3405–3420.

Jazwinski, A.H., 1970. Stochastic Processes and Filtering Theories. Academic Press.

Kalman, R.E., 1960. A New Approach to Linear Filtering amd Prediction Problems. Trans. ASME - J. Basic Eng. 82 (Series, 35–45.

Kerr, Y.H., Waldteufel, P., Wigneron, J.-P., Delwart, S., Cabot, F., Boutin, J., Escorihuela, M.-J., Font, J., Reul, N., Gruhier, C., Juglea, S.E., Drinkwater, M.R., Hahne, A., Martín-Neira, M., Mecklenburg, S., 2010. The SMOS Mission: New Tool for Monitoring Key Elements of the Global Water Cycle. Proc. IEEE 98, 666–687. doi:10.1109/JPROC.2010.2043032

Kumar, S. V, Reichle, R.H., Harrison, K.W., Peters-Lidard, C.D., Yatheendradas, S., Santanello, J.A., 2012. A comparison of methods for a priori bias correction in soil moisture data assimilation. Water Resour. Res. 48.

Laiolo, P., Gabellani, S., Campo, L., Cenci, L., Silvestro, F., 2015a. Assimilation of remote sensing observations into a continuous distributed hydrological model : impacts on the hydrologic cycle, in: 2015 IEEE International Geoscience and Remote Sensing Symposium (IGARSS), Milan,. pp. 1308–1311. doi:10.1109/IGARSS.2015.7326015

Laiolo, P., Gabellani, S., Campo, L., Silvestro, F., Delogu, F., Rudari, R., Pulvirenti, L., Boni, G., Fascetti, F., Pierdicca, N., Crapolicchio, R., Hasenauer, S., Puca, S., 2015b. Impact of different satellite soil moisture products on the predictions of a continuous distributed hydrological model. Int. J. Appl. Earth Obs. Geoinf. 48. doi:10.1016/j.jag.2015.06.002

Leroux, D.J., Kerr, Y.H., Bitar, A.A., Bindlish, R., Jackson, T.J., Berthelot, B., Portet, G., 2014. Comparison between SMOS, VUA, ASCAT, and ECMWF soil moisture products over four watersheds in U.S. IEEE Trans. Geosci. Remote Sens. 52. doi:10.1109/TGRS.2013.2252468

Leroux, D.J., Pellarin, T., Vischel, T., Cohard, J.M., Gascon, T., Gibon, F., Mialon, A., Galle, S., Peugeot, C., Seguis, L., 2016. Assimilation of SMOS soil moisture into a distributed hydrological model and impacts on the water cycle variables over the Ouémé catchment in Benin. Hydrol. Earth Syst. Sci. 20, 2827–2840. doi:10.5194/hess-20-2827-2016

Li, Y., Ryu, D., Western, A.W., Wang, Q.J., Robertson, D.E., Crow, W.T., 2014. An integrated error parameter estimation and lag-aware data assimilation scheme for real-time flood forecasting. J. Hydrol.

Lievens, H., De Lannoy, G.J.M., Al Bitar, A., Drusch, M., Dumedah, G., Hendricks Franssen, H.J., Kerr, Y.H., Tomer, S.K., Martens, B., Merlin, O., Pan, M., Roundy, J.K., Vereecken, H., Walker, J.P., Wood, E.F., Verhoest, N.E.C., Pauwels, V.R.N., 2016. Assimilation of SMOS soil moisture and brightness temperature products into a land surface model. Remote Sens. Environ. 180, 292–304. doi:10.1016/j.rse.2015.10.033

Lievens, H., Tomer, S.K.K., Al Bitar, A., De Lannoy, G.J.M.J.M., Drusch, M., Dumedah, G., Hendricks Franssen, H.-J.J., Kerr, Y.H.H., Martens, B., Pan, M., Roundy, J.K.K., Vereecken, H.,

Walker, J.P.P., Wood, E.F.F., Verhoest, N.E.C.E.C., Pauwels, V.R.N.R.N., 2015. SMOS soil moisture assimilation for improved hydrologic simulation in the Murray Darling Basin, Australia. Remote Sens. Environ. 168, 146–162. doi:10.1016/j.rse.2015.06.025

Liu, Y., Weerts, A.H., Clark, M., Hendricks Franssen, H.J., Kumar, S., Moradkhani, H., Seo, D.J., Schwanenberg, D., Smith, P., Van Dijk, A.I.J.M., Van Velzen, N., He, M., Lee, H., Noh, S.J., Rakovec, O., Restrepo, P., 2012. Advancing data assimilation in operational hydrologic forecasting: Progresses, challenges, and emerging opportunities. Hydrol. Earth Syst. Sci. 16, 3863–3887.

Liu, Y.Y., Dorigo, W.A., Parinussa, R.M., De Jeu, R.A.M., Wagner, W., McCabe, M.F., Evans, J.P., Van Dijk, A.I.J.M., 2012. Trend-preserving blending of passive and active microwave soil moisture retrievals. Remote Sens. Environ. 123, 280–297.

Loizu, J., Álvarez-Mozos, J., Casalí, J., Goñi, M., 2016. Evaluation of TOPLATS on three Mediterranean catchments. J. Hydrol. 539, 141–161. doi:10.1016/j.jhydrol.2016.05.025

Loosvelt, L., Vernieuwe, H., Pauwels, V.R.N., De Baets, B., Verhoest, N.E.C., 2014. Local sensitivity analysis for compositional data with application to soil texture in hydrologic modelling. Hydrol. Earth Syst. Sci. 17, 461–478.

López López, P., Wanders, N., Schellekens, J., Renzullo, L.J.L.J., Sutanudjaja, E.H.E.H., Bierkens, M.F.P.M.F.P., 2016. Improved large-scale hydrological modelling through the assimilation of streamflow and downscaled satellite soil moisture observations. Hydrol. Earth Syst. Sci. 20, 3059–3076. doi:10.5194/hess-20-3059-2016

Lü, H., Crow, W.T., Zhu, Y., Ouyang, F., Su, J., 2016. Improving streamflow prediction using remotely-sensed soil moisture and snow depth. Remote Sens. 8. doi:10.3390/rs8060503

Lucau-Danila, C., Callens, M., Defourny, P., Verhoest, N.E.C., Pauwels, V.R.N., 2005. Vegetation parameter retrieval from SAR data using near-surface soil moisture estimates dereived from a hydrological model, in: Owe, M., D'Urso, G. (Eds.), Proceedings of SPIE - The International Society for Optical Engineering. pp. 597603-597603–12. doi:10.1117/12.627574

Massari, C., Brocca, L., Tarpanelli, A., Moramarco, T., 2015. Data Assimilation of Satellite Soil Moisture into Rainfall-Runoff Modelling: A Complex Recipe? Remote Sens. 7, 11403–11433.

doi:10.3390/rs70911403

Masseroni, D., Cislaghi, A., Camici, S., Massari, C., Brocca, L., 2017. A reliable rainfall-runoff model for flood forecasting: Review and application to a semi-urbanized watershed at high flood risk in Italy. Hydrol. Res. 48. doi:10.2166/nh.2016.037

Matgen, P., Fenicia, F., Heitz, S., Plaza, D., de Keyser, R., Pauwels, V.R.N., Wagner, W., Savenije, H., 2012a. Can ASCAT-derived soil wetness indices reduce predictive uncertainty in well-gauged areas? A comparison with in situ observed soil moisture in an assimilation application. Adv. Water Resour. 44, 49–65.

Matgen, P., Heitz, S., Hasenauer, S., Hissler, C., Brocca, L., Hoffmann, L., Wagner, W., Savenije, H.H.G., 2012b. On the potential of MetOp ASCAT-derived soil wetness indices as a new aperture for hydrological monitoring and prediction: A field evaluation over Luxembourg. Hydrol. Process. 26, 2346–2359.

Melone, F., Neri, N., Morbidelli, R., Saltalippi, C., 2001. A conceptual model for flood prediction in basins of moderate size. Appl. Simul. Model. In: Hamza, 461–6.

Milly, P.C.D., 1986. Event-based simulation model of moisture and energy fluxes at bare soil surface. Water Resour. Res. 22, 1680–1692.

Moradkhani, H., Hsu, K.-L., Gupta, H., Sorooshian, S., 2005. Uncertainty assessment of hydrologic model states and parameters: Sequential data assimilation using the particle filter. Water Resour. Res. 41. doi:10.1029/2004WR003604

Moradkhani, H., Sorooshian, S., Gupta, H.V. V, Houser, P.R.R., 2005. Dual state-parameter estimation of hydrological models using ensemble Kalman filter. Adv. Water Resour. 28, 135–147. doi:10.1016/j.advwatres.2004.09.002

Naeimi, V., Scipal, K., Bartalis, Z., Hasenauer, S., Wagner, W., 2009. An Improved Soil Moisture Retrieval Algorithm for ERS and METOP Scatterometer Observations. IEEE Trans. Geosci. Remote Sens. 47, 1999–2013. doi:10.1109/TGRS.2008.2011617

Nash, J.E., Sutcliffe, J. V, 1970. River flow forecasting through conceptual models part I - A discussion of principles. J. Hydrol. 10, 282–290.

NRCS-USDA, 2014. 12th Edition Keys to Soil Taxonomy.

Owe, M., de Jeu, R., Holmes, T., 2008. Multisensor historical climatology of satellite-derived global land surface moisture. J. Geophys. Res. F Earth Surf. 113.

Parrens, M., Zakharova, E., Lafont, S., Calvet, J.C., Kerr, Y., Wagner, W., Wigneron, J.P., 2012. Comparing soil moisture retrievals from SMOS and ASCAT over France. Hydrol. Earth Syst. Sci. 16, 423–440.

Passerat De Silans, A., Vauclin, M., Bruckler, L., Bertuzzi, P., Brunet, Y., 1986. Numerical modeling of water and heat flows in unsaturated soils under atmospheric excitation. Comparison with field data, in: Heat Transfer, Proceedings of the International Heat Transfer Conference. pp. 2629–2634.

Paulik, C., Dorigo, W., Wagner, W., Kidd, R., 2014. Validation of the ASCAT soil water index using in situ data from the International Soil moisture network. Int. J. Appl. Earth Obs. Geoinf. 30, 1–8.

Pauwels, V.R.N., De Lannoy, G.J.M., 2009. Ensemble-based assimilation of discharge into rainfall-runoff models: A comparison of approaches to mapping observational information to state space. Water Resour. Res. 45, n/a-n/a. doi:10.1029/2008WR007590

Pauwels, V.R.N., Hoeben, R., Verhoest, N.E.C., De Troch, F.P., 2001. The importance of the spatial patterns of remotely sensed soil moisture in the improvement of discharge predictions for small-scale basins through data assimilation. J. Hydrol. 251, 88–102.

Pauwels, V.R.N., Hoeben, R., Verhoest, N.E.C., De Troch, F.P., Troch, P.A., 2002. Improvement of TOPLATS-based discharge predictions through assimilation of ERS-based remotely sensed soil moisture values. Hydrol. Process. 16, 995–1013.

Pauwels, V.R.N., Wood, E.F., 1999. A soil-vegetation-atmosphere transfer scheme for the modeling of water and energy balance processes in high latitudes 2. Application and validation. J. Geophys. Res. D Atmos. 104, 27823–27839.

Pauwels, V.R.N.V.R.N., Verhoest, N.E.C.N.E.C.N.E.C., De Lannoy, G.J.M.G.J.M.G.J.M., Guissard, V., Lucau, C., Defourny, P., 2007. Optimization of a coupled hydrology-crop growth model through the assimilation of observed soil moisture and leaf area index values using an ensemble Kalman filter. Water Resour. Res. 43, n/a-n/a. doi:10.1029/2006WR004942

Peters-Lidard, C.D., Zion, M.S., Wood, E.F., 1997. A soil-vegetation-atmosphere transfer scheme for modeling spatially variable water and energy balance processes. J. Geophys. Res. D Atmos. 102, 4303–4324.

Philip, J.R., 1957. The theory of infiltration, 4, Sorptivity and algebraic infiltration equations. Soil Sci. 84, 257–264.

Plaza, D.A., De Keyser, R., De Lannoy, G.J.M., Giustarini, L., Matgen, P., Pauwels, V.R.N., 2012. The importance of parameter resampling for soil moisture data assimilation into hydrologic models using the particle filter. Hydrol. Earth Syst. Sci. 16, 375–390.

Qiu, J., Crow, W.T., Mo, X., Liu, S., 2014. Impact of temporal autocorrelation mismatch on the assimilation of satellite-derived surface soil moisture retrievals. IEEE J. Sel. Top. Appl. Earth Obs. Remote Sens. 7. doi:10.1109/JSTARS.2014.2349354

Randrianasolo, A., Thirel, G., Ramos, M.H.H., Martin, E., 2014. Impact of streamflow data assimilation and length of the verification period on the quality of short-term ensemble hydrologic forecasts. J. Hydrol. 519, Part, 2676–2691. doi:http://dx.doi.org/10.1016/j.jhydrol.2014.09.032

Reichle, R.H., 2004. Bias reduction in short records of satellite soil moisture. Geophys. Res. Lett. 31, L19501. doi:10.1029/2004GL020938

Reichle, R.H., Crow, W.T., Keppenne, C.L., 2008. An adaptive ensemble Kalman filter for soil moisture data assimilation. Water Resour. Res. 44.

Reichle, R.H.H., Koster, R.D., 2004. Bias reduction in short records of satellite soil moisture. Geophys. Res. Lett. 31, L19501. doi:10.1029/2004GL020938

Reichle, R.H.H., McLaughlin, D.B.B., Entekhabi, D., 2002. Hydrologic data assimilation with the ensemble Kalman filter. Mon. Weather Rev. 130, 103–114.

Renzullo, L.J., van Dijk, A.I.J.M., Perraud, J.M., Collins, D., Henderson, B., Jin, H., Smith, A.B., McJannet, D.L., 2014. Continental satellite soil moisture data assimilation improves root-zone moisture analysis for water resources assessment. J. Hydrol.

Rötzer, K., Montzka, C., Bogena, H., Wagner, W., Kerr, Y.H., Kidd, R., Vereecken, H., 2014. Catchment scale validation of SMOS and ASCAT soil moisture products using hydrological

modeling and temporal stability analysis. J. Hydrol. 519, 934–946.

Ryu, D., Crow, W.T., Zhan, X., Jackson, T.J., 2009. Correcting unintended perturbation biases in hydrologic data assimilation. J. Hydrometeorol. 10, 734–750.

Sahoo, A.K., De Lannoy, G.J.M., Reichle, R.H., Houser, P.R., 2013. Assimilation and downscaling of satellite observed soil moisture over the Little River Experimental Watershed in Georgia, USA. Adv. Water Resour. 52, 19–33. doi:10.1016/j.advwatres.2012.08.007

Scipal, K., Holmes, T., De Jeu, R., Naeimi, V., Wagner, W., 2008. A possible solution for the problem of estimating the error structure of global soil moisture data sets. Geophys. Res. Lett. 35.

SCS - Soil Conservation Service., 1972. National Engineering Handbook, section 4. Washington D.C.

Sivapalan, M., Beven, K., Wood, E.F., 1987. On hydrologic similarity. 2. A scaled model of storm runoff production. Water Resour. Res. 23, 2266–2278.

Stoffelen, A., 1998. Toward the true near-surface wind speed: Error modeling and calibration using triple collocation. J. Geophys. Res. C Ocean. 103.

Su, C.-H., Ryu, D., 2015. Multi-scale analysis of bias correction of soil moisture. Hydrol. Earth Syst. Sci. 19. doi:10.5194/hess-19-17-2015

Su, C.-H., Ryu, D., Crow, W.T., Western, A.W., 2014. Beyond triple collocation: Applications to soil moisture monitoring. J. Geophys. Res. 119. doi:10.1002/2013JD021043

Thiboult, A., Anctil, F., 2015. On the difficulty to optimally implement the Ensemble Kalman filter: An experiment based on many hydrological models and catchments. J. Hydrol. 529, 1147–1160. doi:10.1016/j.jhydrol.2015.09.036

Trudel, M., Leconte, R., Paniconi, C., 2014. Analysis of the hydrological response of a distributed physically-based model using post-assimilation (EnKF) diagnostics of streamflow and in situ soil moisture observations. J. Hydrol. 514, 192–201.

Wagner, W., Hahn, S., Kidd, R., Melzer, T., Bartalis, Z., Hasenauer, S., Figa-Saldaña, J., De Rosnay, P., Jann, A., Schneider, S., Komma, J., Kubu, G., Brugger, K., Aubrecht, C., Züger, J., Gangkofner, U., Kienberger, S., Brocca, L., Wang, Y., Blöschl, G., Eitzinger, J., Steinnocher, K., Zeil, P., Rubel, F., 2013. The ASCAT Soil Moisture Product: A Review of its Specifications, Validation Results, and Emerging Applications. Meteorol. Zeitschrift 22, 5–33.

doi:10.1127/0941-2948/2013/0399

Wagner, W., Lemoine, G., Rott, H., 1999. A method for estimating soil moisture from ERS Scatterometer and soil data. Remote Sens. Environ. 70, 191–207.

Wanders, N., Bierkens, M.F.P., de Jong, S.M., de Roo, A., Karssenberg, D., 2014a. The benefits of using remotely sensed soil moisture in parameter identification of large-scale hydrological models. Water Resour. Res. 50, 6874–6891. doi:10.1002/2013WR014639

Wanders, N., Karssenberg, D., Bierkens, M., Parinussa, R., de Jeu, R., van Dam, J., de Jong, S., 2012. Observation uncertainty of satellite soil moisture products determined with physically-based modeling. Remote Sens. Environ. 127, 341–356.

Wanders, N., Karssenberg, D., De Roo, A., de Jong, S.M., Bierkens, M.F.P., 2014b. The suitability of remotely sensed soil moisture for improving operational flood forecasting. Hydrol. Earth Syst. Sci. 18, 2343–2357. doi:10.5194/hess-18-2343-2014

Wang, T., Franz, T.E., You, J., Shulski, M.D., Ray, C., 2017. Evaluating controls of soil properties and climatic conditions on the use of an exponential filter for converting near surface to root zone soil moisture contents. J. Hydrol. 548. doi:10.1016/j.jhydrol.2017.03.055

Xie, X., Zhang, D., 2010. Data assimilation for distributed hydrological catchment modeling via ensemble Kalman filter. Adv. Water Resour. 33, 678–690.

Xu, X., Tolson, B.A., Li, J., Staebler, R.M., Seglenieks, F., Haghnegahdar, A., Davison, B., 2015. Assimilation of SMOS soil moisture over the Great Lakes basin. Remote Sens. Environ. 169, 163–175. doi:10.1016/j.rse.2015.08.017

Yan, H., Moradkhani, H., 2016. Combined assimilation of streamflow and satellite soil moisture with the particle filter and geostatistical modeling. Adv. Water Resour. 94, 364–378. doi:10.1016/j.advwatres.2016.06.002

Yilmaz, M.T., Crow, W.T., 2013. The Optimality of Potential Rescaling Approaches in Land Data Assimilation. J. Hydrometeorol. 14, 650–660. doi:10.1175/JHM-D-12-052.1

Zeng, J., Li, Z., Chen, Q., Bi, H., Qiu, J., Zou, P., 2015. Evaluation of remotely sensed and reanalysis soil moisture products over the Tibetan Plateau using in-situ observations. Remote Sens. Environ. 163, 91–110. doi:10.1016/j.rse.2015.03.008

Fig. 1. Catchment location, topography, hydrological features and instrumentation.

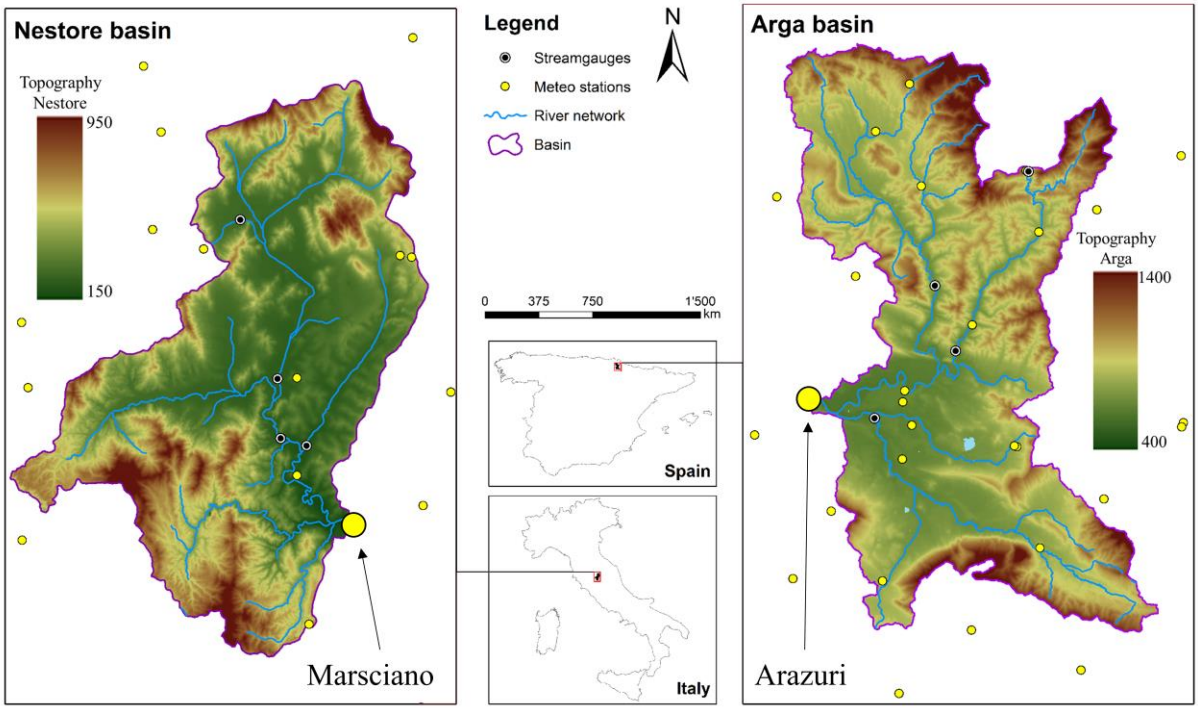

Fig. 2. ASCAT grid overlaid on a) the Nestore catchment and b) the Arga catchment.

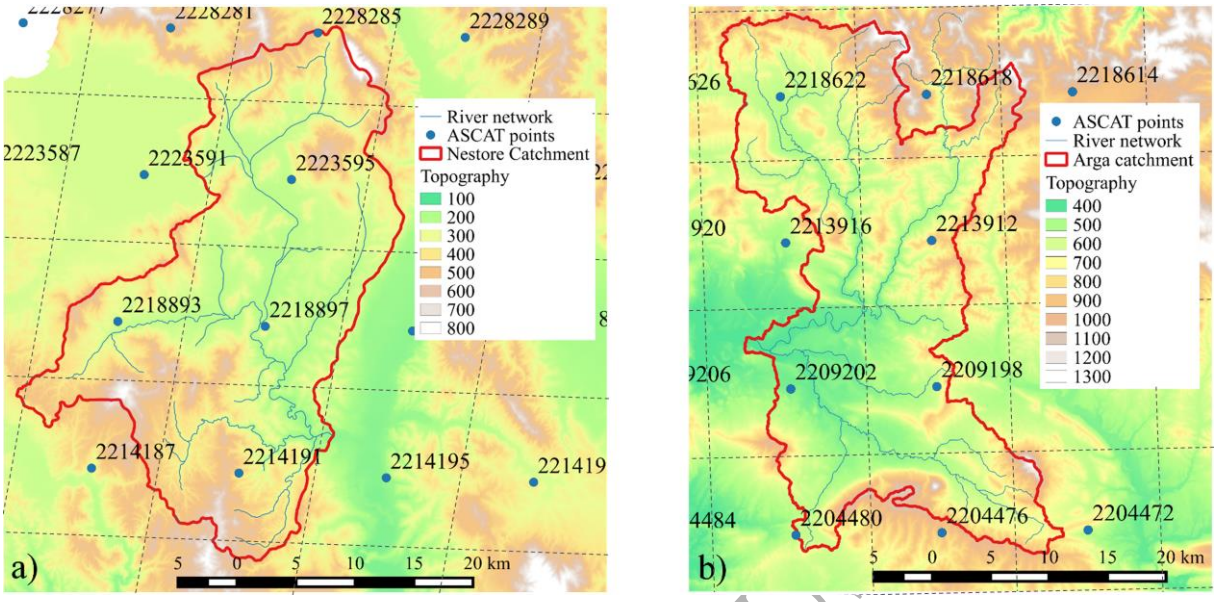

Fig. 3. MISDc and TOPLATS modeling schemes. MISDc adapted from (Brocca et al., 2011) and TOPLATS scheme adapted from (Loizu et al., 2016). The three main modeling processes of each model are detailed: plot 3a shows the soil-water balances (SWB), plot 3b the main runoff generating mechanism characteristic of each mode, and plot 3c shows the runoff routing included in each model. Water balance budgets in the TOPLATS scheme: precipitation (P), net precipitation (P_n), evaporation (E), infiltration excess runoff (q_{ie}), saturation excess runoff (q_s), baseflow (q_{bf}), infiltration (I), drainage (g) and capillary rise (w), where vegetated soil (vg), wet canopy (wc) and bare soils (bs) are distinguished in subscripts.

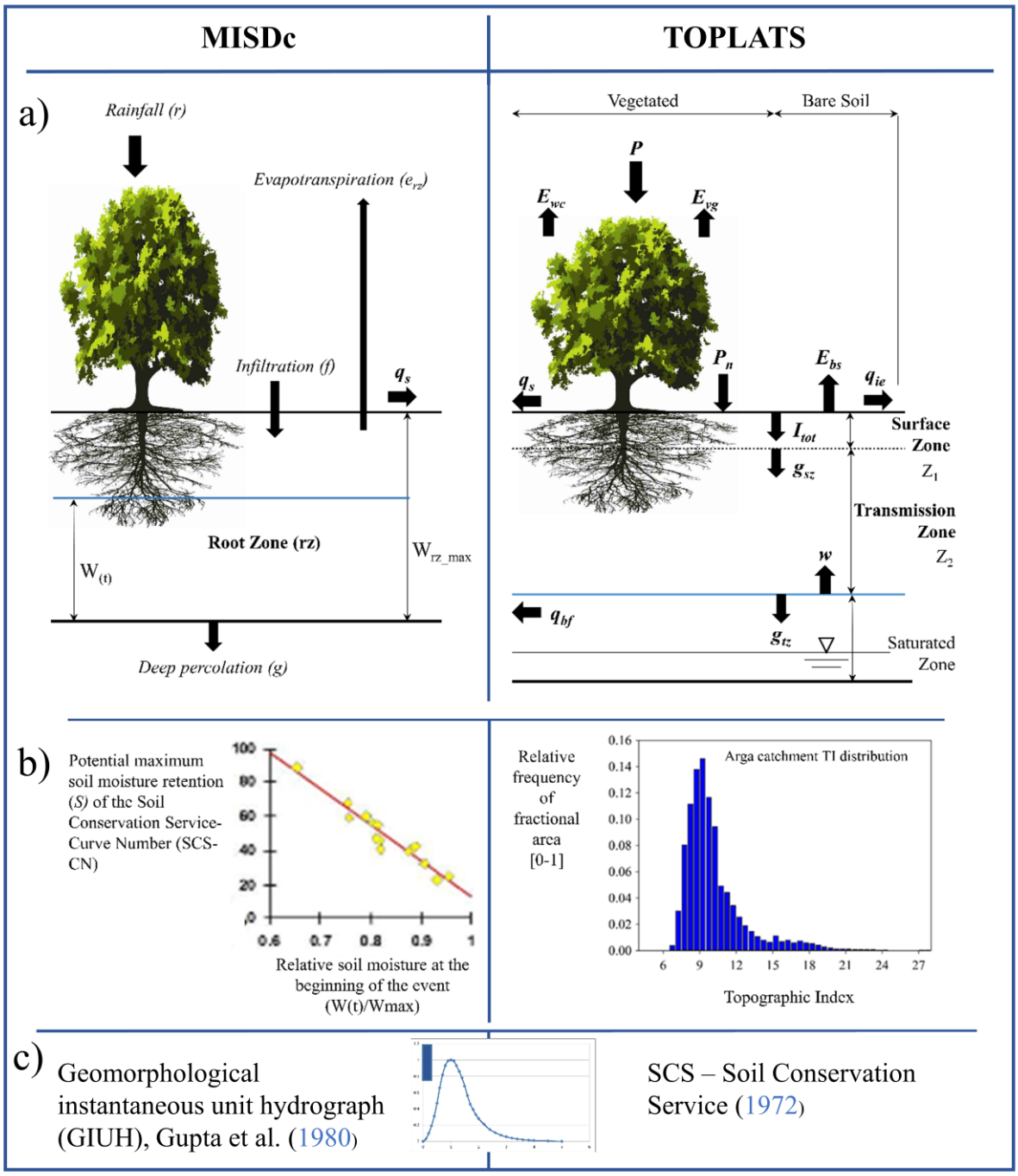
MISDc
TOPLATS
a)
Rainfall (r)
Evapotranspiration (e_{rz})
Infiltration (f)
q_s
Root Zone (rz)
$W_{(t)}$
W_{rz_max}
Deep percolation (g)
Vegetated
Bare Soil
P
E_{wc}
E_{vg}
P_n
E_{bs}
q_{ie}
I_{tot}
Surface Zone
Z_1
g_{sz}
Transmission Zone
Z_2
w
q_{bf}
g_{tz}
Saturated Zone
b)
Potential maximum soil moisture retention (S) of the Soil Conservation Service-Curve Number (SCS-CN)
Relative soil moisture at the beginning of the event (W(t)/Wmax)
Relative frequency of fractional area [0-1]
Arga catchment TI distribution
Topographic Index
c)
Geomorphological instantaneous unit hydrograph (GIUH), Gupta et al. (1980)
SCS – Soil Conservation Service (1972)

Fig. 4. Model calibration and validation: a) Nestore catchment and b) Arga catchment results. Time series and scatter plots of calibration and validation periods (separated through a dotted vertical line in the upper plots).

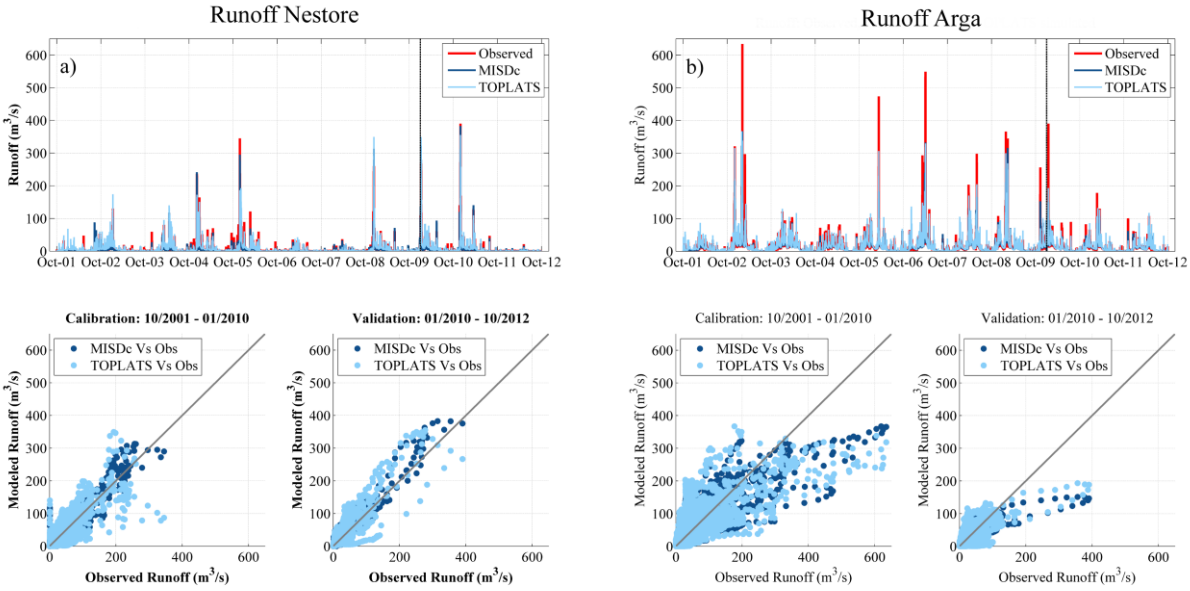

Fig. 5. The SWI re-scaling technique (CDF, LR and VM) results for MISDc (a-d) and TOPLATS (e-f). Plots a, b, e and f correspond to the Nestore catchment, and plots c, d, g and h to Arga. Plots on the left represent the calibration period, and those on the right the validation period. Note that only co-located simulated and observed values are shown in the plots to avoid misinterpretations of the soil moisture dynamics.

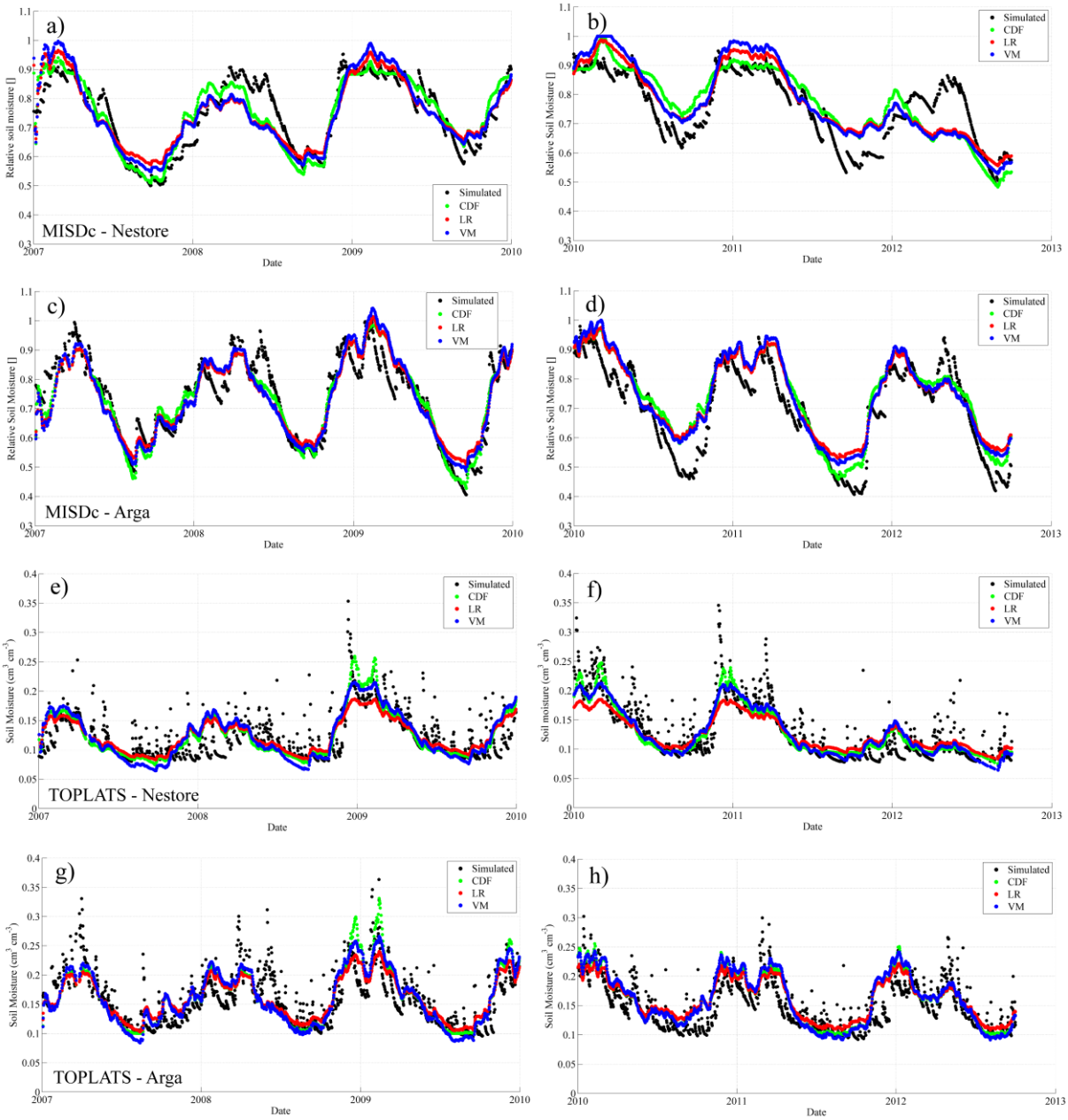

Fig. 6. Scatterplots of re-scaled SWIs (with CDF, LR and VM methods) and simulated SSM values with MISDc (a-d) and TOPLATS (e-h).

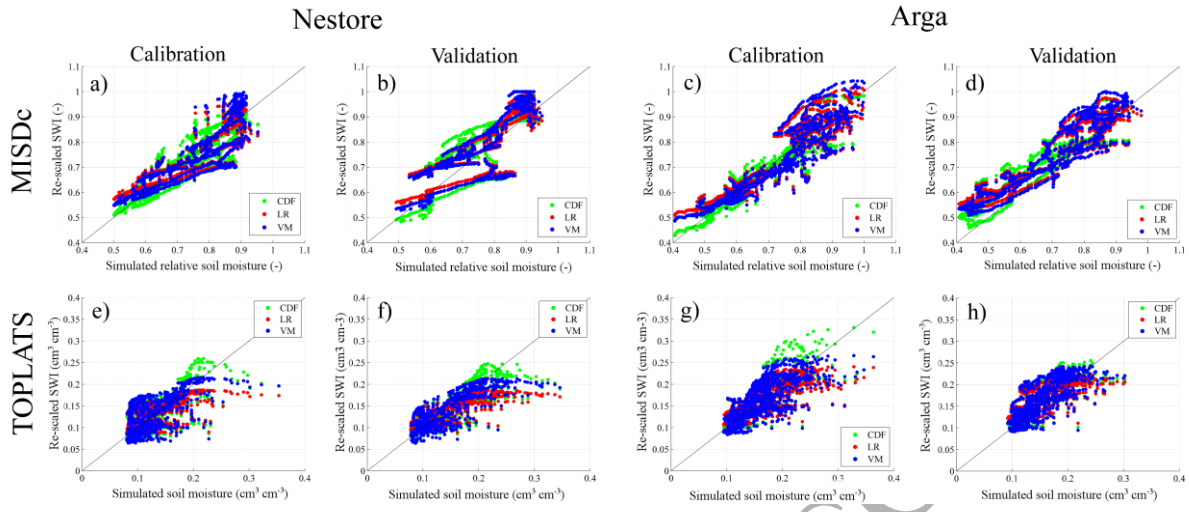

Fig. 7. MISDc and TOPLATS models' streamflow and surface soil moisture (SSM) ensembles: a) Nestore catchment using MISDc, b) Arga catchment using MISDc, c) Nestore catchment using TOPLATS and, d) Arga catchment using TOPLATS. The ensembles are represented by their 5-95 percentile range. Soil moisture in MISDc is expressed as saturation degree [0-1], whereas in TOPLATS is expressed in volumetric units (cm^3 cm^{-3}).

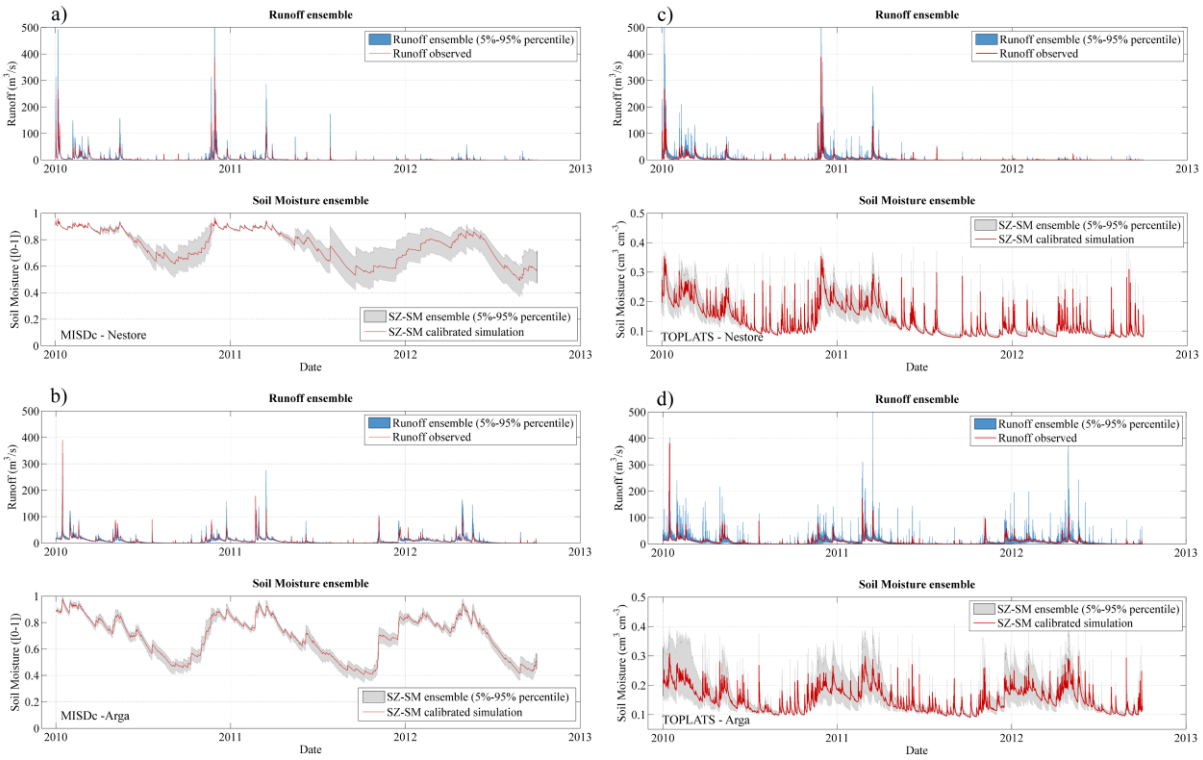

Fig. 8. Streamflow simulation efficiency after DA using MISDc and TOPLATS models. MISDc results for the Nestore (a, c, e, and g plots) and Arga (b, d, f, and h plots) catchments are shown on the left columns. TOPLATS results for the Nestore (i, k, m, and o plots) and Arga (j, l, n, and p plots) catchments are shown on the right columns. Four efficiency evaluation criteria results are shown: NSE (plots a, b, i and j), Pbias (c, d, k and l), Eff_{OL} (e, f, m and n) and NRMSE (g, h, o and p). Horizontal axes correspond to the assumed ASCAT observation error values. Colors correspond to different SWI re-scaling techniques. In NSE and Pbias plots (a, b, c, d, i, j, k and l) the solid horizontal line indicates the Val results, and the dotted line indicates the OL results (Table 2).

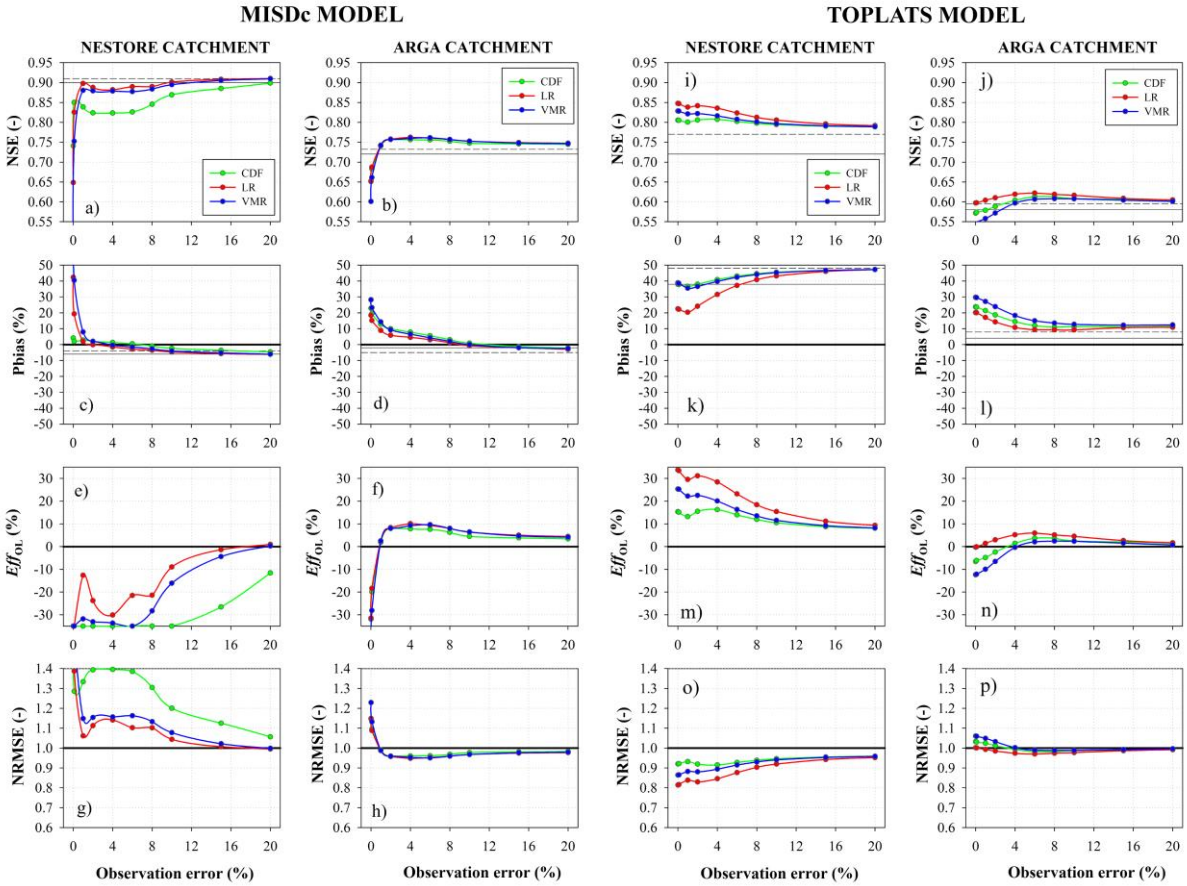

Fig. 9. MISDc (a and b plots) and TOPLATS (c and d plots) model assimilation results for the Nestore (a and c) and Arga (b and d) catchments. Three plots are presented per catchment: (i) observed, validation and DA time series, (ii) error between observed and validation series and (iii) error reduction achieved after DA, where positive values indicate error reduction. Results shown in this figure are those obtained with the best DA set-up, as detailed in Table 2 for each model and catchment combination.

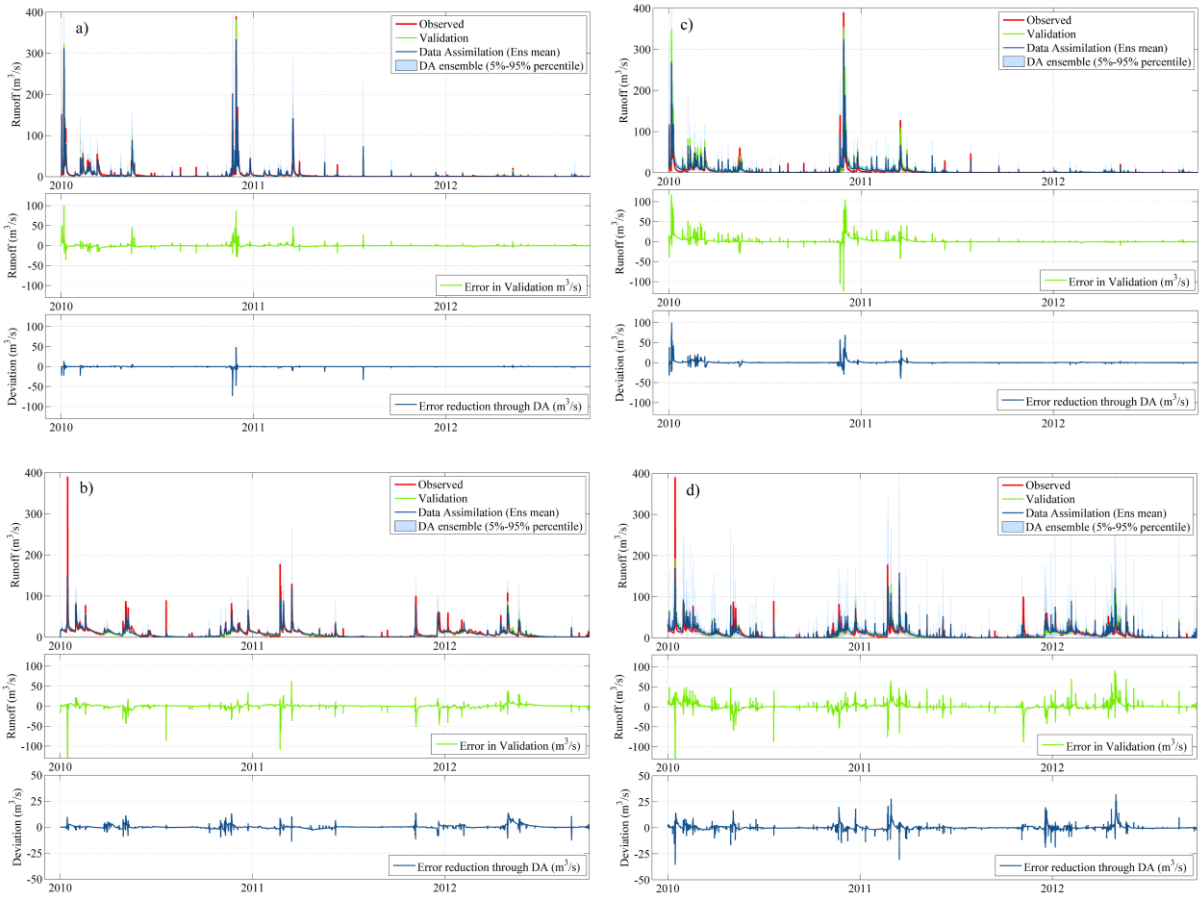

Fig. 10. Efficiency variation (Eff_{Val}) compared to validation time series for the Nestore (a and c) and Arga catchments (b and d). The MISDc model results are shown in plots a and b, while the TOPLATS results are presented in plots c and d.

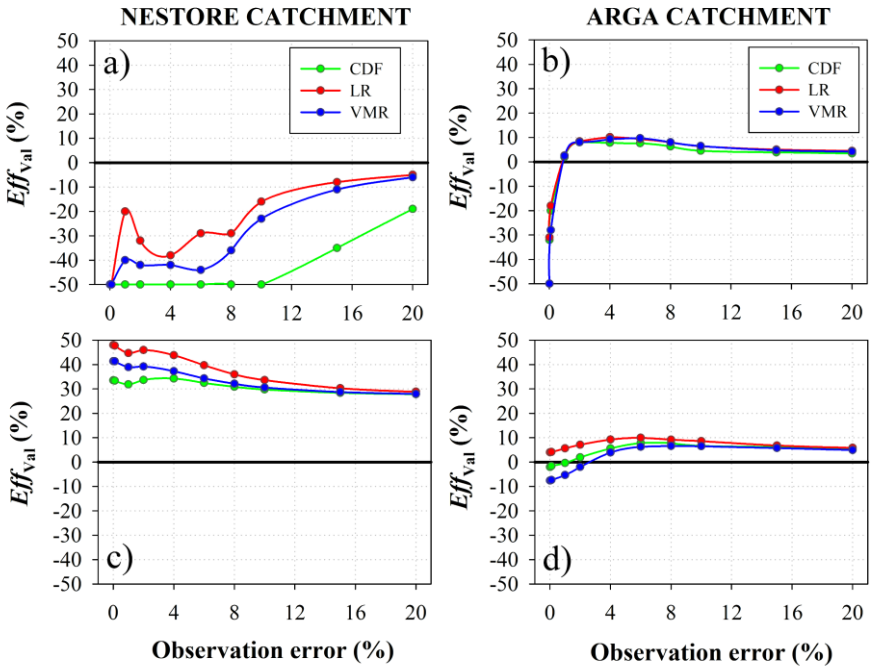

Fig. 11. Monthly variation (expressed as monthly m^3/s) in simulation accuracy after DA in the validation period for a) Nestore using MISDc, b) Arga using MISDc, c) Nestore using TOPLATS and d) Arga using TOPLATS. Positive values (in green) indicate that simulation after DA increased the accuracy of the total monthly simulated streamflow volume. Negative values (in red) indicate a reduction in the simulation accuracy. Monthly results also correspond to best set-up conditions, as detailed in Table 2 (For Nestore using MISDc, LR and 4% observation errors were used).